Energy Nexus 17 (2025) 100357

Contents lists available at ScienceDirect

Energy Nexus

journal homepage: www.elsevier.com/locate/nexus

Full Length Article

Thermal analysis and optimal fluid selection for the novel integrated vapor compression cycle and ORC system for ultra-low grade waste heat recovery using the desuperheating method

Muhammad Asim [a,*], Sheheryar Khan [a], Shahid Ali Khan [b], Taha Baig [a], Muhammad Imran [c], Abdul Wasy Zia [d], Fahid Riaz [e], Michael K.H. Leung [f]

[a] Division of Science, Engineering, and Health Studies (SEHS), School of Professional Education & Executive Development, The Hong Kong Polytechnic University, Hong Kong
[b] Department of Mechanical Engineering, City University of Hong Kong, Hong Kong
[c] Department of Mechanical, Biomedical and Design Engineering, Aston University, Birmingham B4 7ET, UK
[d] Institute of Mechanical, Process, and Energy Engineering (IMPEE), School of Engineering and Physical Sciences, Heriot-Watt University, Edinburgh EH14 4AS, UK
[e] College of Engineering, Abu Dhabi University, Abu Dhabi, United Arab Emirates
[f] Ability R&D Energy Research Centre, School of Energy and Environment, City University of Hong Kong, Hong Kong, PR China

ARTICLE INFO

Keywords:
Vapor compression cycle
Organic Rankine cycle
Ultra-low grade
Waste heat recovery
Desuperheating method
Thermodynamic analysis

ABSTRACT

This research investigates the thermal performance and working fluid selection from ultra-low-grade waste heat recovery. The study examines the desuperheating method of a novel integrated Vapor Compression Cycle (VCC) and the organic Rankine Cycle (ORC) system for electricity generation. Two cooling methods are analysed and compared, water-cooled VCC-water-cooled ORC and air-cooled VCC -air-cooled ORC. The study was conducted on a vapor compression system with 35-kW refrigeration capacity and evaluated various performance indices. The results indicate that for the water-water cooled system, R407c-R141b is the potential working fluid, achieving an overall coefficient of performance (COP_{sys}) of 3.20, ORC thermal efficiency of 7.56 %, and net electricity output of 0.28 kW. R410a-R141b is recommended in the air-air-cooled system due to its higher ORC thermal efficiency (7.67 %) than the water-water-cooled system (7.56 %), resulting in a power output of 0.44 kW. Sensitivity analysis reveals that desuperheating is preferable for obtaining higher ORC thermal efficiency. Increasing the condensing water temperature improves net electricity and ORC thermal efficiency. Furthermore, a higher mass flow rate of condensing water enhances system COP and system exergy efficiency but decreases ORC thermal efficiency.

Nomenclature

A_i	total heat exchanger area	*Acronyms*	
$a_{r,l}$	all-liquid non-boiling transfer coefficient	AC	air-conditioning
B_o	boiling number	COP	coefficient of performance
E	electricity, kW	ESR	electricity saving rate, kW
E_{net}	net electricity, kW	LMTD	logarithmic mean temperature diff.,K
E_{gen}	generated electricity	ODP	ozone depletion potential

(*continued on next column*)

(*continued*)

G	heat exchanger geometric functions	SHX	sharing heat exchanger
		VCC	vapor compression cycle
		WHR	waste heat recovery
h	specific enthalpy, kJ/kg		
I_{evap}	exergy destruction rate, kW		
Pr	Prandtl number		
P_{co}	Heat exchanger pinch		
m_{vcc}	mass flow rate, kg /s		
Nu	Nusselt number		
Re	Reynold number		
s	specific entropy, kJ/(kg·K)		

(*continued on next page*)

* Corresponding author.
E-mail address: muhammad.asim@cpce-polyu.edu.hk (M. Asim).

https://doi.org/10.1016/j.nexus.2024.100357

Available online 29 December 2024

(*continued*)

T	temperature, °C
T_3	condenser inlet temperature
T_{sg}	saturated vapor temperature, K
T_{indoor}	indoor air temperature
T_0	Dead State Temperature, K
T_3	condenser inlet temperature, K
T_{amb}	ambient air temperature, K
Tsg	Dead State Temperature, K
U	overall heat transfer coefficient
V	volumetric flow rate, m^3/s
$\dot{Q}_{in}$	cooling capacity, kW
$\dot{Q}_{superheat}$	high-quality waste heat, kW
$\dot{Q}_{reco,dw}$	recovered waste heat rate, kW
$\dot{Q}_{out}$	condenser heat rate, kW
x	refrigerant quality
Greek symbols	
η_{th}	thermal efficiency
β	chevron angle, radian
μ	dynamic viscosity, Ns/m^2
Subscripts	
1–15	state points
evap	evaporator
f	full condensing
g	generator
i	region part
wall	wall of the heat exchanger

1. Introduction

Global warming, climate change, ozone depletion, and air pollution have profoundly influenced global energy policy. Because of these pressing environmental concerns, there has been a notable increase in research efforts to find efficient ways to utilize energy resources. One area of focus in recent years has been utilizing low-temperature waste heat from sources such as solar, geothermal, waste heat, and biomass. Harnessing this low-temperature waste heat reduces reliance on conventional and non-renewable power generation methods. This shift towards utilizing low-temperature waste heat offers a more sustainable approach to energy production and alleviates the associated environmental consequences [1]. Efficiently recovering waste or low-temperature heat sources can have a substantial impact on reducing greenhouse gas emissions and enhancing overall energy efficiency. Waste heat is generated in various contexts, including industrial processes, heavy-duty vehicles, and renewable energy sources such as biomass, solar, and geothermal. By effectively harnessing and utilizing this waste heat, we can minimize the release of harmful greenhouse gases into the atmosphere while maximizing the productive use of energy resources. This comprehensive approach helps combat climate change and promotes sustainable energy practices across different sectors, contributing to a greener and more efficient future [2]. Waste heat energy, which would otherwise be lost to the environment, holds significant potential as a carbon replacement. Waste heat can be harnessed through efficient recovery and utilization without generating additional emissions. This research highlights the importance of capturing and utilizing waste heat as a sustainable alternative to conventional energy sources, contributing to emission reductions and optimizing energy efficiency [3]. In tropical regions, approximately 25 % of the overall electrical energy consumption is attributed to a combination of residential, commercial, and industrial buildings [4]. Air conditioning accounts for the majority of energy consumption in households, making it the most significant contributor. During the summer, approximately 30–50 % of the electricity supplied to urban areas is dedicated to power air conditioning systems [5]. The condenser rejects low-grade heat in air-conditioning and refrigeration systems, typically at 65 °C or lower temperatures. Despite previous efforts to develop and implement technologies for recovering waste heat below 200 °C, a significant amount of low-grade energy, particularly below 100 °C, is currently being wasted and discarded as heat, leading to thermal and general environmental pollution [6]. The waste heat generated by air conditioning systems is considered a low-grade thermal energy source. Still, it is underutilized and <10 % effectively reused due to the limited demand for hot water in Hong Kong. Developing technologies that fully harness and utilize this waste heat is critical to enhance air conditioning system performance and minimize environmental impact. Conversion of waste heat into electricity can be achieved convincingly by applying thermodynamic approaches. The waste heat from an air conditioning system belongs to a closed heat source [7]. Numerous strategies and thermodynamic cycles have been explored to recover waste heat effectively. The Organic Rankine Cycle (ORC) has emerged as a highly promising technology among these approaches. The ORC functions on a principle similar to the conventional steam Rankine cycle but with a notable distinction: it employs organic compounds as the working fluid instead of steam. This utilization of organic compounds offers distinct advantages due to their lower boiling points than water. Consequently, the ORC can effectively extract energy from low-temperature heat sources that would otherwise be challenging to harness using conventional energy conversion technologies. These heat sources encompass a wide range, including solar energy, geothermal reservoirs, and waste heat generated by diverse industrial processes. The ORC provides a practical and efficient solution for tapping into this previously untapped energy potential, enabling the recovery of valuable resources from what would have otherwise been wasted heat [8–10].

In tropical regions, a significant portion (nearly 56 %) of the energy consumed in buildings is attributed to air conditioning purposes. In recent studies, researchers have explored the integration of the vapor compression cycle with the organic Rankine cycle, aiming to investigate the thermodynamic behavior and performance of the integrated system. In one of the configurations, the compressor of the VCC system is driven by the organic Rankine cycle (ORC) system. Both cycles share common condensers and the same working fluid for their operation. An external heat source has been used to drive the ORC cycle. The heat source temperature, evaporation, and condensing temperatures of these cycles for thermodynamic modeling vary from 60 °C - 300 °C, −15 °C - 15 °C and 30 °C - 55 °C. Overall system coefficient of performance (COP), mass flow rate/cooling capacity, and turbine/compressor sizing parameters were used as performance indicators to assess the thermodynamic response of the VCC—ORC system [11–15]. The vapor compression refrigeration cycle (VCC) is the most commonly used air-conditioning cycle. In this cycle, the condenser releases significant heat at a low temperature into the environment. However, an organic Rankine cycle (ORC) can efficiently recover this waste heat to generate electricity. Implementing this technology holds great market potential and can substantially reduce energy consumption in residential and industrial settings. Previous research studies investigated integrating the Organic Rankine Cycle (ORC) system with the vapor compression cycle. However, in these studies, the heat input to the ORC system has primarily been sourced from an external heat source. In some configurations, the work generated by the expander in the ORC system has even been utilized to drive the compressor of the vapor compression cycle (VCC) system. Zhang et al. [16] optimized a Carnot refrigerator's performance parameters with heat recovery (CRHR). Increasing the heat recovery reservoir outlet temperature improved refrigerating rates and reduced input power but decreased the refrigeration coefficient, heat recovery coefficient, comprehensive coefficient, and exergy efficiency. Optimal performance was achieved at a heat recovery heat exchanger area ratio of 1.0, enabling complete recycling of condensing heat. Tang et al. [17] conducted simulations and optimization analyses involving nine working fluids and two heat sources. They investigated four unique cycles to determine the optimal combination of working fluids, system

configurations, and operating parameters to maximize system efficiency. Their research focused on the correlation between system performance and the position of the pinch point (PP), which plays a pivotal role in heat matching. Prigmore and Barber [18] developed the ORC and VCC integrated system prototype. The system employed an ORC system utilizing R113 as the working fluid, seamlessly connected to an R12 VCC system and a generator. The primary objective of their research was to achieve a dual outcome: delivering a substantial 3-ton capacity for residential cooling while simultaneously generating 1 kW of electricity. To achieve this impressive feat, the ORC system was ingeniously designed to harness the abundant heat provided by solar energy sources. Taufique et al. [19]. conducted a study on solar energy technology to optimize the organic Rankine cycle using 4-E analysis and prioritized three refrigerants (R-113, R-11, and R-1233zd). Considering critical factors such as solar irradiance and turbine inlet temperature, the study achieved a 54.58 % improvement in energy efficiency, a 68 % reduction in power/cost of electricity, and a 16 % increase in ecological efficiency. This hybrid system offers cheaper and more sustainable electricity generation. Braimakis et al. [20]. investigated the energy efficiency of three regenerative Organic Rankine Cycle (ORC) configurations by assessing various working fluid options. They conducted a comparative analysis against simple regenerative ORCs and identified a specific configuration that demonstrated a substantial improvement in efficiency. Comparing organic compounds and mixtures is another crucial aspect of ORC design [21,22]. Onyeocha et al. [23] developed a tetrafluoroethane (R134a) refrigerator-waste heat recovery dryer for tropical regions. The system used a retrofitted condenser unit as the heat recovery mechanism and achieved a maximum drying temperature of 49 °C. The system effectively recovered and utilized waste heat with a specific moisture extraction rate of 0.19–0.22 kg/hr and an energy utilization ratio of 0.92. It offers the potential for simultaneous refrigeration and heating applications, benefiting agriculture and laundry businesses. Computer-aided molecular design (CAMD) is commonly used for working fluid design in the ORC [24–27]. However, predefining the ORC configuration limits the exploration and comparison of ORC performance with different working fluids. The optimization of the heat exchange network (HEN) has been a longstanding concern in this regard [28].The maximum system COP of 0.71 has been achieved with a warm water temperature of 102 °C. Nasir et al. [29] designed an ORC-driven VCC system tailored to domestic air conditioning applications. They assessed the system's thermal performance by considering seven working fluids and their combinations within the integrated setup. A hot water source at 100 °C was utilized as the heat input. Among the various combinations analyzed, the configuration combining R134a as the working fluid for the ORC system and Isobutane for the VCC system demonstrated the highest level of performance. This configuration achieved a maximum combined coefficient of performance (COP) of 0.281. S. Aphornratana and T. Sriveerakul [12] conducted a theoretical analysis on the coupling of a Vapor Compression Cycle (VCC) and an Organic Rankine Cycle (ORC) with an expander-compressor unit. The working fluids chosen for the system were R22 and R134a. The integrated system utilized a shared working fluid and condenser. The system's coefficient of performance (COP) varies between 0.1 and 0.6, with generator and condenser temperatures ranging from 60 to 90 °C and 30–50 °C. F. Moles et al. [1] analyzed the integration of the organic Rankine cycle (ORC) and vapor compression cycle (VCC) system, with a specific focus on utilizing low-temperature heat sources and working fluids that have a low global warming potential. They assessed the thermal and electrical Coefficients of Performance (COPs) of the combined system, which were found to vary between 0.30 and 1.10 for thermal COP and 15 to 110 for electrical COP, respectively. Their analysis concluded that the optimal working fluids for the integrated ORC-VCC system were HFO-1336mzz (Z) and HFO-1234ze (E). Asim et al. [30] proposed an integrated air-conditioning-organic Rankine cycle (i-AC—ORC) system for efficient waste heat recovery. R600a-R123 is identified as the optimal fluid pair for the integrated system. The i-VCC—ORC system improves the combined COP from 3.10 to 3.54. The organic Rankine cycle subsystem achieves a net electricity generation of 1.41 kW with a thermal efficiency of 3.05 % and an exergy efficiency of 39.30 %. The study also analyzes the system's performance under varying external conditions. In another study conducted by Asim et al. [31], performance evaluation and working fluid selection for an integrated vapor compression cycle-organic Rankine cycle (i-VCC—ORC) system has been carried out. R600a-R141b achieves a net COP of 3.54 and ORC thermal efficiency of 3.05 %. Integrating the VCC with the ORC increases system COP by 12.5 % compared to the standalone VCC. Kim KH and Perez-Blanco [3] performed a comprehensive thermodynamic analysis of a combined Organic Rankine Cycle (ORC) and Vapor Compression Cycle (VCC) system. The study focused on using the same working fluids for power generation and refrigeration. Isobutane was specifically selected for sensitivity analysis due to its high thermal efficiency. The results demonstrated that the integrated system effectively utilized low-grade thermal energy with temperatures surpassing 90 °C. Furthermore, the ORC and VCC systems achieved a minimum cooling temperature of 5 °C. In the study conducted by Saleh [15], a parametric analysis was performed on an integrated ORC-VCC system. This system included a shared condenser, and the power generated by the expander was utilized to drive the compressor and pump. The system was powered by a low-temperature heat source operating at around 100 °C, and ten different working fluids were evaluated. Among the options considered, R600 emerged as the optimal working fluid. It demonstrated a coefficient of performance (COP) of up to 0.718 at a condenser temperature of 30 °C, achieving the lowest total mass flow rate. D.K. Kim et al. [6] performed a detailed parametric evaluation of an organic Rankine cycle (ORC) system that utilized low-grade waste heat below 80 °C. The selected working fluid for the system was R245fa. The results demonstrated that the ORC system could generate 411.3 W of power with an efficiency of 3.6 % when operating at a heat source temperature of 80 °C. Zhao et al. [32] conducted a comprehensive comparative analysis of system parameters using different working fluids to harness low-grade waste heat at 85 °C. Their investigation concluded that R123 exhibited superior performance as a working fluid, showing notable thermal efficiency and turbine power output. This finding highlights R123 as an effective choice for optimizing energy conversion in systems utilizing low-grade waste heat. Similarly, Lakew et al. [33] compared the performance of Organic Rankine Cycle (ORC) systems employing various working fluids. The analysis revealed that R227ea demonstrated suitability for heat sources within the temperature range of 80–160 °C. In both studies, energetic and exergetic analyses were conducted, and the resulting findings served as effective approaches to evaluate system performance. These analyses provided valuable insights into key parameters for the investigated ORC systems.

The efficient recovery of low-temperature waste heat in vapor compression cycle (VCC) systems using the desuperheating method has yet to be extensively explored, particularly in achieving high conversion efficiency. However, there is considerable potential in effectively recovering high-quality heat from the VCC condenser, as it can enhance both the combined coefficient of performance (COP) of the air-conditioning system and the thermal efficiency of the organic Rankine cycle (ORC) system. This promising approach offers significant benefits, including reducing waste heat, improving the commercial viability of waste heat recovery in air conditioning systems, mitigating greenhouse gas emissions, and contributing to sustainable development.

This research paper proposes a novel integrated system called the integrated vapor compression cycle and organic Rankine cycle (i-VCC—ORC) to recover low-grade waste heat using the desuperheating approach. The distinctive aspect of this configuration lies in the fact that the waste heat rejected by the condenser of the VCC cycle drives the ORC, allowing the recovered waste heat to be utilized for electricity production. The primary focus of this study is on the design, selection of working fluids, and performance evaluation of the i-VCC—ORC system. The performance of the system is assessed based on metrics such as COP,

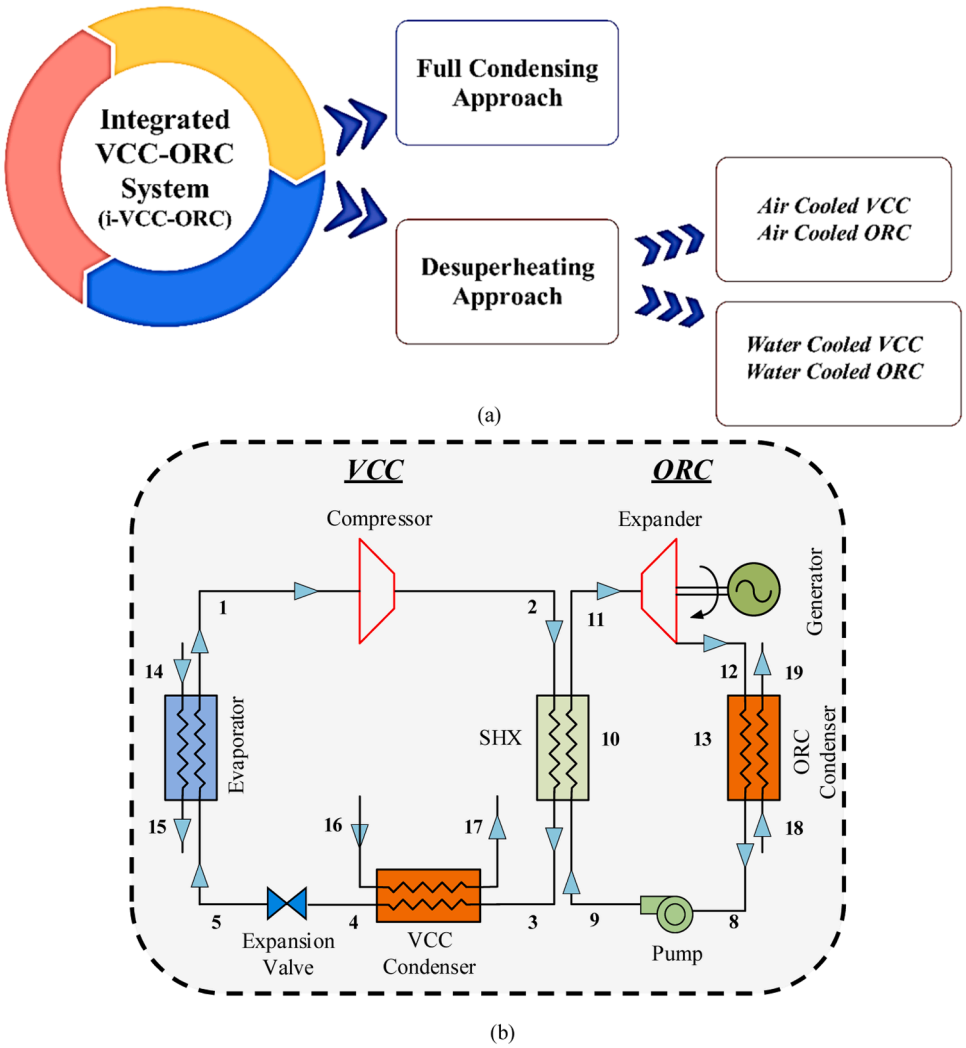

Fig. 1. (a) Waste heat recovery approaches (b) Schematic diagram for a desuperheating method for heat recovery.

cycle thermal efficiency, and exergy efficiency. By analyzing and optimizing these performance indicators, the researchers aim to demonstrate the potential of the i-VCC—ORC system in efficiently recovering waste heat and producing electricity, thereby contributing to enhanced energy utilization and sustainable practices in the air conditioning industry. This novel approach addresses the challenge of low-temperature waste heat recovery in VCC systems and offers significant potential for improving energy efficiency, reducing waste, and promoting sustainable development. The findings of this study have the potential to significantly advance the field of waste heat recovery, offering valuable insights for developing and implementing efficient, sustainable, and environmentally friendly air conditioning systems.

2. System description

2.1. Desuperheating approach for ultra-low-grade waste heat recovery

This section presents an integrated system that combines the vapour compression cycle (VCC) and organic Rankine cycle (ORC) to recover ultra-low-grade waste heat effectively. The study focuses on a specific method for recovering waste heat from high-quality superheated regions within the VCC system, illustrated in Fig. 1(a). A detailed discussion of this method is presented, focusing on the use of different cooling media for the VCC and ORC condensers. In the full condensing method [31], the waste heat from the VCC condenser is fully recovered and utilized in the ORC system in the shared heat exchanger (SHX) for electricity production [30,31] and the condensers (VCC and ORC) reject heat at ambient temperature. Therefore, a new integration has been proposed in which the high-quality heat from the superheated region of the VCC cycle is recovered and utilized in the SHX. Fig. 1 shows the configuration of an integrated VCC—ORC system in which heat is recovered from high-quality vapor from a superheated region (desuperheating approach). A portion of high-quality waste heat (state points 2–3) is recovered from the superheated region, and the remaining heat (state points 3–4) is recovered in a VCC condenser by cooling water/ambient air (state points 3–4). High-quality waste heat (state points 2–3) is much smaller than the heat recovered from the full condensation technique. Consequently, the exhaust indoor air can serve as the cooling medium in the organic Rankine Cycle (ORC) condenser. Compared to the conventional heat recovery method, the desuperheating approach employed by the vapor compression cycle (VCC) system introduces a two-stage heat rejection process. This approach involves recovering a portion of high-quality superheated vapor through a sharing heat exchanger (SHX) known as a desuperheater. This recovered vapor serves as the driving heat source for the organic Rankine cycle (ORC) system. The remaining waste heat is then released in the VCC condenser.

The study investigates two configurations: the water-water-cooled integrated VCC—ORC system and the air-air-cooled integrated VCC—ORC system. These configurations utilize different cooling fluids (water or air) in the VCC condenser. The study thoroughly discusses the

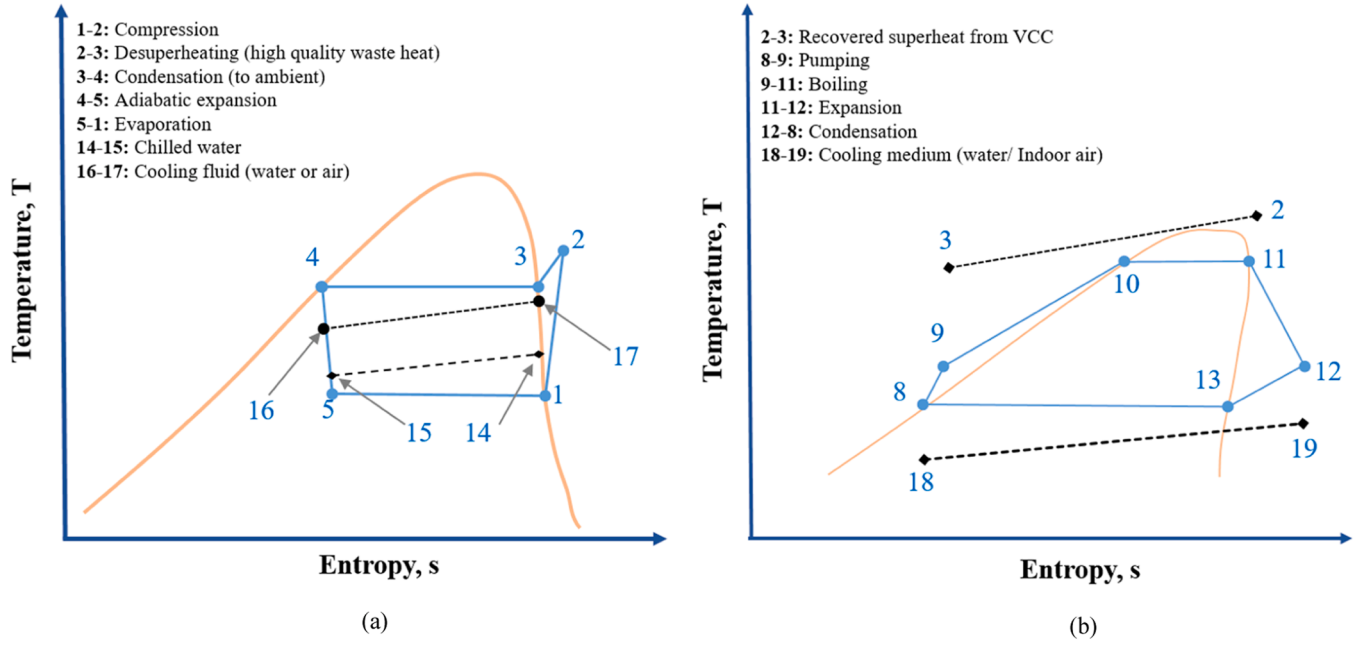

Fig. 2. Temp-entropy diagrams for (a) the VCC cycle and (b) The ORC cycle.

Table 1
Selected working fluids properties [20,15].

System	Working fluids	Mol. Mass (kg/kmol)	Critical Temp. (°C)	Critical Pressure (MPa)	Ozone Depletion Potential	Global Warming Potential
VCC	R134a	102.03	101.1	4.06	0	1430
	R290	44.10	96.7	4.25	0	20
	R404A	97.60	72.0	3.72	0	3900
	R407C	86.20	85.8	4.60	0	1800
	R600a	58.12	134.7	3.63	0	20
	R410A	72.58	70.5	4.81	0	2100
ORC	Butane	58.12	152.0	3.80	0	20
	R141b	116.95	204.4	4.21	0.12	725
	R227ea	170.03	102.8	3.00	0	3220
	R245fa	134.05	154.0	3.65	0	1030
	R1233zd(e)	130.49	166.5	3.62	0.00034	7

impact of various parameters including ORC condensing air/water temperature, mass flow rate, VCC chilled water temperature, and indoor air temperature on system coefficient of performance (COP), standalone COP of the VCC system, net electricity generation, ORC thermal efficiency, system exergy efficiency, and system and component exergy destruction for both the water-water-cooled integrated VCC—ORC and air-air-cooled integrated VCC—ORC systems. The temperature-entropy (T-s) diagrams for both configurations are shown in Fig. 2(a) and (b).

3. Selection of working fluid

Several critical factors must be considered when selecting suitable working fluids for the integrated VCC—ORC system. These include the fluids' physical and chemical properties, such as their fouling potential, corrosiveness, toxicity, and flammability. Additionally, it is essential to ensure that the selected fluids are fully compatible with the system's operational conditions. [34].

It is crucial to address environmental concerns using working fluids in the system that have low global warming potential (GWP) and ozone depletion potential (ODP). To align with the established practices in the refrigeration and cryogenic industry, a set of six refrigerants (R134a, R290, R404A, R407C, R600a, and R410A) has been identified as potential working fluids for the vapor compression cycle (VCC) subsystem. In a study conducted by Bao et al. [35], working fluids were categorized based on different heat source temperatures, leading to the identification of five dry and isentropic fluids (butane, R141b, R227ea, R245fa, and R1233zd(e)) as potential candidates for the organic Rankine cycle (ORC) subsystem. These fluids were chosen considering their suitability for the ORC process. Table 1 presents a comprehensive overview of the thermal properties, ozone depletion potential (ODP), and global warming potential (GWP) of these potential working fluids, providing valuable information for the selection process.

4. Research methodology

The integrated VCC—ORC cycle introduces an innovative method for waste heat recovery. By implementing a sharing heat exchanger (SHX), we can recover waste heat from the VCC condenser and utilize it in the ORC cycle. The SHX serves a dual role, acting as the VCC condenser and the ORC evaporator. Instead of recovering the entire heat rejection from the VCC condenser, this unique configuration focuses on recovering a portion of the waste heat. The remaining waste heat is then released to the ambient environment, making this a promising approach for waste heat management.

The waste heat recovery process involves the utilization of high-quality waste heat from the superheated region of the VCC through the desuperheating method. On the other hand, the remaining waste heat is directed to the VCC condenser, which is cooled either by water or by air, resulting in heat rejection at the ambient temperature. This waste heat recovery concept incorporates using two different cooling media

Table 2
Design conditions for Water-water cooled integrated VCC—ORC system.

Item	Unit	Value
Cooling capacity	kW	35.0
Cooling water temperature	°C	35.0
Indoor air temperature	°C	25.0
Dead state temperature	°C	25.0
Ambient air temperature	°C	35.0
Chilled water pressure	MPa	0.101
Cooling water pressure	MPa	0.101
Exhaust indoor air pressure	MPa	0.101
η_{comp}	(%)	75
η_{pump}	(%)	80
$\eta_{expander}$	(%)	75
$\eta_{generator}$	(%)	95
$m_{chilled\ water}$	(kg/s)	1.7
$m_{cooling\ air}$	(kg/s)	4.0

Table 3
Design conditions for Air-air cooled integrated VCC—ORC system.

Item	Unit	Value
Cooling capacity	kW	35.0
Ambient air temperature	°C	35.0
Exhaust indoor air temperature	°C	25.0
Dead state temperature	°C	25.0
Chilled water pressure	MPa	0.101
Cooling water pressure	MPa	0.101
Exhaust indoor air pressure	MPa	0.101
η_{comp}	(%)	75
η_{pump}	(%)	80
$\eta_{expander}$	(%)	75
$\eta_{generator}$	(%)	95
UA value - VCC evaporator	kW/K	4.8
UA value - SHX	kW/K	0.80
UA value - VCC condenser	kW/K	3.5
UA value - ORC condenser	kW/K	7.0
$m_{chilled\ water}$	(kg/s)	1.7
$m_{cooling\ air}$	(kg/s)	4.0

for the ORC and VCC condensers to dissipate heat into the surrounding environment. If the VCC condenser and ORC condensers are cooled by water, the system is classified as a water-water-cooled integrated VCC—ORC (water-water-cooled system). Conversely, if the VCC condenser is cooled by water and the ORC condenser is cooled by indoor exhaust air, it is referred to as an air-air-cooled integrated VCC—ORC system (air-air-cooled system). The system configuration assumes the employment of counter-flow-type heat exchangers.

A VCC system with a refrigeration capacity of 10 tons (35 kW) is considered to assess the system's performance. A thermodynamic model of the integrated system has been created and implemented using the Engineering Equation Solver (EES) [36]. This model facilitates evaluating and examining the system's performance, enabling a comprehensive analysis of the integrated VCC—ORC cycle. Additionally, it allows for investigating waste heat recovery and effective energy utilization within the system. The thermodynamic analyses of the system are carried out based on several assumptions: steady-state operation, the use of different working fluids in the VCC and ORC cycles, neglecting friction and heat loss, and disregarding changes in kinetic/potential energy as well as pressure drops in heat exchangers and pipe work. Additional assumptions include the VCC working fluid entering the compressor as a saturated vapor and exiting the condenser as a saturated liquid, adiabatic expansion in the VCC, the ORC working fluid exiting the condenser as a saturated liquid and entering the expander as a saturated vapor, and assuming no superheating at the exit of the ORC evaporator (SHX). These assumptions provide a simplified framework for analyzing the thermodynamic performance and characteristics of the system. As discussed earlier, in a water-water-cooled integrated VCC—ORC system, the superheated waste heat from the VCC condenser is utilized by the ORC evaporator in SHX as the heat source for electricity generation. Cooling water is used as the heat sink for cooling the ORC condenser. Based on the operating conditions, the design criteria is given in Table 2 below.

Similarly, in an air-air-cooled integrated VCC—ORC system, the ORC evaporator as the heat source utilizes the superheated waste heat from the VCC condenser for electricity generation. Ambient air is used as the heat sink for cooling the VCC condenser, and indoor exhaust air is used for cooling the ORC condenser. Based on the actual operating conditions, the design criteria are given in Table 3

4.1. Model validation

To ensure the developed thermodynamic model's accuracy and reliability, it is validated by comparing it with established models from published literature. Due to the limitations of directly validating the integrated model, the individual VCC and ORC models are validated separately using relevant literature sources. The VCC model is validated by comparing it to the conditions presented in the study by O. Badr et al. [37]. specifically for the isentropic refrigerant R22. Similarly, the validation of the ORC model is based on the work conducted by B.F. Tchanche [38]Through this validation process, the credibility and effectiveness of the thermodynamic model were ensured, allowing it to represent the behavior and performance of the integrated system accurately.

The validation of the VCC system against O. Badr et al. [37] is presented in Fig. 3. The validation process involves assessing parameters such as the COP of the standalone VCC, compressor work, and refrigeration effect. The VCC system operates under specific conditions, including a VCC condensing temperature of 40 °C, a compressor isentropic efficiency of 70 %, and an evaporating temperature of −20 °C. The temperature differences between the evaporator and high-temperature reservoir and between the condenser and low-temperature reservoir remain constant at 5 °C. This validation focuses on examining the influence of the VCC system's condensing temperature on the VCC COP, compressor work, and refrigeration effect, with the isentropic refrigerant R22 being utilized.

To validate the ORC model, a selection of three dry refrigerants (RC318, R114, and R600) and one isentropic refrigerant (R141b) is chosen. These refrigerants are compared to the present study for a power output of 2 kW. Table 4 presents the input data used by B.F. Tchanche et al. [38] for model verification. The validation process involves comparing various parameters, including the inlet and outlet pressures of the expander (P_{min} and P_{max}), the mass flow rate of the working fluid (m_{wf}), thermal efficiency, exergy efficiency, and total exergy destruction in the ORC system. The validation results in Table 5 closely agree with the findings published in B.F. Tchanche et al. [38], with percentage variations <1 % for dry and isentropic refrigerants. Consequently, these validated models can be integrated for ultra-low-grade waste heat recovery for the proposed desuperheating method.

4.2. Thermodynamic modeling

The thermodynamic equations used to develop a thermodynamic model for water-water-cooled and air-air-cooled integrated VCC—ORC systems are identical in their generalized form for energetic analysis. However, due to the different cooling media for the VCC and ORC condensers, the exergetic analysis varies between the two systems. The thermodynamic equations for the water-water and air-air-cooled integrated VCC—ORC systems are provided below.

The VCC condenser inlet temperature (T_3) for VCC refrigerant is preliminarily designed by:

$$T_3 = n(T_2 - T_{sg}) + T_{sg} \quad (1)$$

Where n is any number between 0 and 1, T_{sg} is the saturated vapour

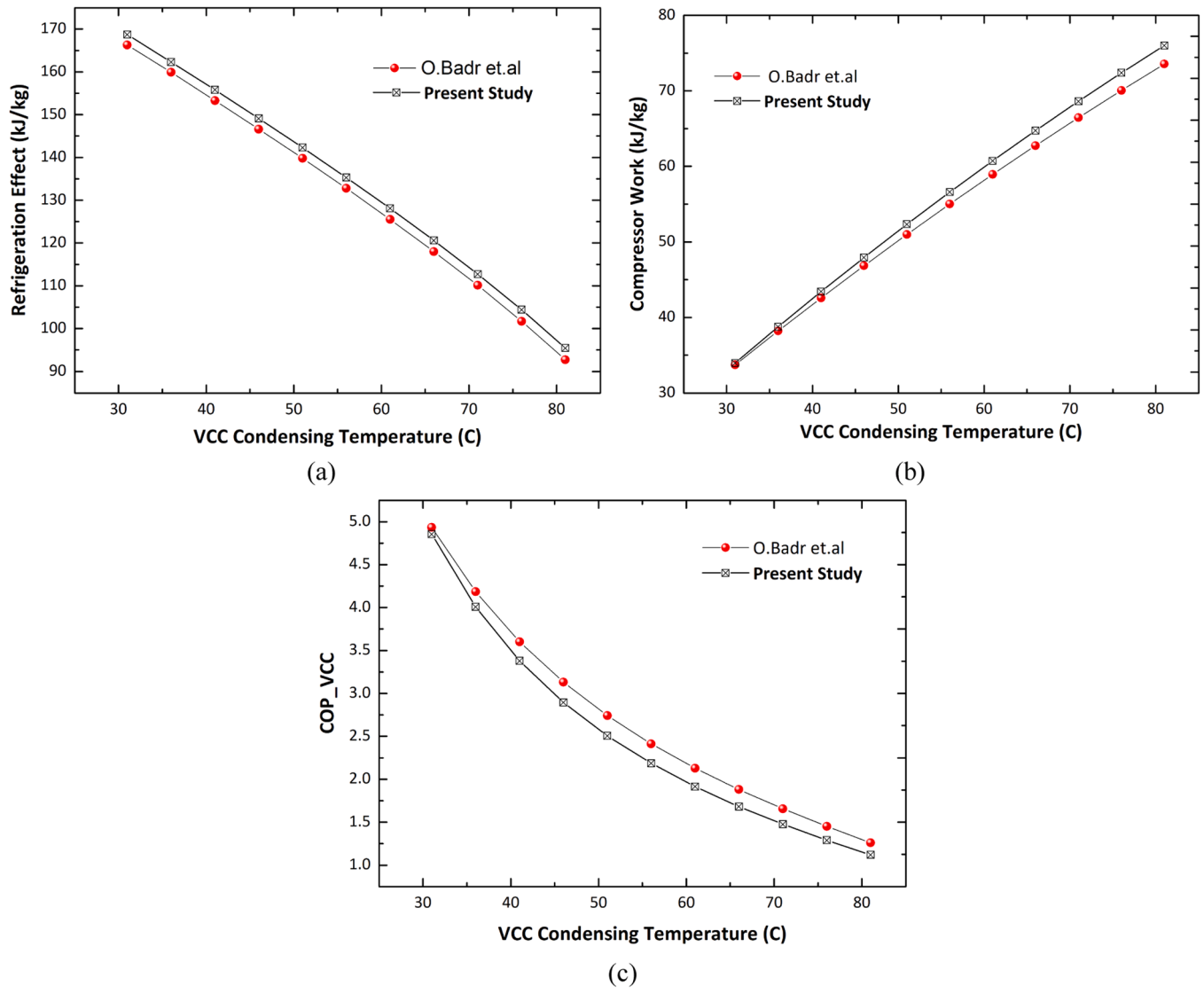

Fig. 3. (a) VCC Condensing temperature vs Refrigeration effect for R22; (b) Condensing temperature vs Compressor work for R22. (c) VCC condensing temperature vs VCC COP for R22.

Table 4
ORC model validation data from [38].

Parameter	Symbol	Value
Evaporation temperature	T_e	75 °C
Condensation temperature	T_c	35 °C
Expander isentropic efficiency	η_{exp}	0.70
Pump efficiency	η_{pump}	0.80
Expander mechanical efficiency	η_m	0.63

temperature on the VCC high-pressure side.

The mass flow rate of exhaust indoor air ($\dot{m}_{\mathrm{ex,air}}$) is given by:

$$\dot{m}_{\mathrm{ex,air}} = \frac{\dot{Q}_{\mathrm{in}}}{C_{p_{air}}(T_{\mathrm{amb}} - T_{\mathrm{indoor}})} \tag{2}$$

Where $\dot{Q}_{\mathrm{in}}$ is the cooling capacity, $C_{p_{air}}$ is the specific heat of air, T_{amb} is the outdoor ambient temperature, and T_{indoor} is the indoor air temperature.

Table 5
ORC model verification with the present study.

Refrigerant	Type	Comparison	P_{min} kPa	P_{max} kPa	m_{wf} kg/s	Thermal Efficiency %	Variation in thermal efficiency %
RC318	Dry	[38]	420	1200	0.38	3.72	0.27
		Present Study	419	1195	0.41	3.71	
R600	Dry	[38]	329	907	0.108	4.24	0.24
		Present Study	327	904	0.109	4.23	
R141b	Isentropic	[38]	112	371	0.173	4.53	0.66
		Present Study	111	372	0.174	4.56	

4.2.1. Energetic analysis

Based on the T-s diagram of VCC shown in Fig. 2(a), the cooling capacity ($\dot{Q}_{\text{in,dw}}$), the compressor work($\dot{W}_{comp,\text{dw}}$), the recovered waste heat rate ($\dot{Q}_{reco,\text{dw}}$), the rejected waste heat rate ($\dot{Q}_{waste,\text{dw}}$), and the initial COP of the VCC subsystem ($COP_{\text{ini,dw}}$) can be expressed as follows:

$$\dot{Q}_{\text{in}} = \dot{m}_{\text{VCC}}(h_1 - h_5) \tag{3}$$

$$\dot{W}_{\text{comp}} = \dot{m}_{\text{VCC}}(h_2 - h_1) \tag{4}$$

$$COP_{VCC} = \frac{\dot{Q}_{in}}{\dot{W}_{comp}}$$

where $\dot{m}_{\text{VCC}}$ is the refrigerant mass flow rate in the VCC system.

Whereas the high-quality waste heat ($\dot{Q}_{\text{superheat}}$) rejected by the VCC cycle is given by

$$\dot{Q}_{\text{superheat}} = \dot{m}_{\text{ORC}}(h_2 - h_3) \tag{5}$$

Meanwhile, the expander power output ($\dot{W}_{\text{turb}}$), the condenser heat rate ($\dot{Q}_{\text{out}}$), the pump work ($\dot{W}_{\text{pump}}$) are expressed as follows:

$$\dot{W}_{\text{exp}} = \dot{m}_{\text{ORC}}(h_{11} - h_{12}) \tag{6}$$

$$\dot{Q}_{\text{out}} = \dot{m}_{\text{ORC}}(h_{12} - h_8) \tag{7}$$

$$\dot{W}_{\text{pump}} = \dot{m}_{\text{ORC}}(h_9 - h_8) \tag{8}$$

where ($\dot{m}_{\text{ORC}}$) is the refrigerant mass flow rate in the ORC subsystem.

Therefore, the generated electricity ($\dot{E}_{\text{gen}}$), the net electricity output ($\dot{E}_{\text{net}}$), the electricity saving rate (ESR) and the thermal efficiency of the ORC subsystem (η_{thermal}) can be written as:

$$\dot{E}_{\text{gen}} = \dot{W}_{\text{exp}} \times \eta_g \tag{9}$$

$$\dot{E}_{\text{net}} = \dot{E}_{\text{gen}} - \dot{W}_{\text{pump}} \tag{10}$$

$$ESR = \frac{\dot{E}_{\text{net}}}{\dot{W}_{\text{comp}}} \tag{11}$$

$$\eta_{\text{thermal}} = \frac{\dot{E}_{\text{net}}}{\dot{Q}_{\text{superheat}}} \tag{12}$$

where (η_g) is the efficiency of the generator.

By applying waste heat recovery, the combined COP of the i-VCC—ORC system ($COP_{\text{comb,dw}}$) can be defined as:

$$COP_{\text{system}} = \frac{\dot{Q}_{\text{in}}}{\dot{W}_{\text{comp}} - \dot{E}_{\text{net}}} \tag{13}$$

4.2.2. Exergetic analysis for water-water cooled integrated VCC—ORC system

An energetic analysis of the performance of the water-water-cooled integrated VCC—ORC system is conducted. The calculation of each component's exergy destruction rate and exergy efficiency is given below.

The exergy destruction rate ($\dot{I}_{\text{evap}}$) and exergy efficiency (η_{evap}) of the evaporator are shown as:

$$\dot{I}_{\text{evap}} = \dot{m}_{\text{VCC}}T_0(s_1 - s_5) + \dot{m}_{\text{CW}}T_0(s_{15} - s_{14}) \tag{14}$$

$$\eta_{\text{evap}} = \frac{\dot{m}_{\text{CW}}[h_{15} - h_{11} - T_0(s_{15} - s_{14})]}{\dot{m}_{\text{VCC}}[h_5 - h_1 - T_0(s_5 - s_1)]} \tag{15}$$

where T_0 is the dead state temperature, ($\dot{m}_{\text{CW}}$) is the mass flow rate of chilled water in the VCC system.

The exergy destruction rate ($\dot{I}_{\text{comp}}$) and exergy efficiency (η_{comp}) of the compressor can be written as:

$$\dot{I}_{\text{comp}} = \dot{m}_{\text{VCC}}T_0(s_2 - s_1) \tag{16}$$

$$\eta_{comp} = \frac{(\dot{W}_{comp} - \dot{I}_{\text{comp}})}{\dot{W}_{comp}} \tag{17}$$

The exergy destruction rate ($\dot{I}_{\text{valve}}$) of the irreversible process in the valve can be represented as:

$$\dot{I}_{\text{valve}} = \dot{m}_{\text{VCC}}T_0(s_5 - s_4) \tag{18}$$

In the SHX, the exergy destruction rate ($\dot{I}_{\text{SHX}}$) and its exergy efficiency (η_{SHX}) are given by:

$$\dot{I}_{\text{SHX}} = \dot{m}_{\text{VCC}}T_0(s_3 - s_2) + \dot{m}_{\text{ORC}}T_0(s_{11} - s_9) \tag{19}$$

$$\eta_{SHX} = \frac{\dot{m}_{\text{VCC}}[h_2 - h_3 - T_0(s_2 - s_3)] - \dot{I}_{\text{SHX}}}{\dot{m}_{\text{VCC}}[h_2 - h_3 - T_0(s_2 - s_3)]} \tag{20}$$

where ($\dot{m}_{\text{ORC}}$) is the refrigerant mass flow rate in the ORC system.

The exergy destruction rate ($\dot{I}_{\text{AC,cond,dw}}$) and exergy efficiency ($\eta_{\text{AC,cond,dw}}$) of the AC condenser can be expressed as:

$$\dot{I}_{\text{VCC,cond}} = \dot{m}_{\text{VCC}}T_0(s_4 - s_3) + \dot{m}_{\text{CW}}T_0(s_{17} - s_{16}) \tag{21}$$

$$\eta_{\text{VCC,cond}} = \frac{\dot{m}_{\text{VCC}}[h_3 - h_4 - T_0(s_3 - s_4)] - \dot{I}_{\text{VCC,cond}}}{\dot{m}_{\text{VCC}}[h_3 - h_4 - T_0(s_3 - s_4)]} \tag{22}$$

Where ($\dot{m}_{\text{CW}}$) is the mass flow rate of cooling water in a VCC condenser.

The expansion process in the expander is irreversible, and the exergy destruction rate ($\dot{I}_{\text{turb}}$) and its exergy efficiency (η_{turb}) is given by:

$$\dot{I}_{\text{turb}} = \dot{m}_{\text{ORC}}T_0(s_{12} - s_{11}) \tag{23}$$

$$\eta_{turb} = \frac{\dot{m}_{\text{ORC}}(h_{11} - h_{12})}{\dot{m}_{\text{ORC}}(h_{11} - h_{12}) + \dot{I}_{\text{turb}}} \tag{24}$$

The exergy destruction rate ($\dot{I}_{\text{cond,dw}}$) and exergy efficiency ($\eta_{\text{ORC,cond,dw}}$) of ORC condenser can be expressed as:

$$\dot{I}_{\text{ORC,cond}} = \dot{m}_{\text{ORC}}T_0(s_8 - s_{12}) + \dot{m}_{\text{CW,ORC}}T_0(s_{19} - s_{18}) \tag{25}$$

$$\eta_{ORC,cond} = \frac{\dot{m}_{\text{ORC}}[h_{12} - h_8 - T_0(s_{12} - s_8)] - \dot{I}_{\text{VCC,cond}}}{\dot{m}_{\text{ORC}}[h_{12} - h_8 - T_0(s_{12} - s_8)]} \tag{26}$$

where ($\dot{m}_{\text{CW,ORC}}$) is the mass flow rate of cooling water in the ORC condenser.

The exergy destruction rate ($\dot{I}_{\text{pump}}$) and exergy efficiency (η_{pump}) of the pump can be defined as:

$$\dot{I}_{\text{pump}} = \dot{m}_{\text{ORC}}T_0(s_9 - s_8) \tag{27}$$

$$\eta_{\text{pump}} = \frac{\dot{m}_{\text{ORC}}(h_9 - h_8) - \dot{I}_{\text{pump}}}{\dot{m}_{\text{ORC}}(h_9 - h_8)} \tag{28}$$

The total exergy destruction ($\dot{I}_{\text{total,dw}}$) in the i-VCC—ORC system is the sum of the exergy destruction in each component, which can be given by Eq. (31):

$$\dot{I}_{\text{total}} = \dot{I}_{\text{SHX}} + \dot{I}_{\text{VCC,cond}} + \dot{I}_{\text{turb}} + \dot{I}_{\text{pump}} + \dot{I}_{\text{evap}} + \dot{I}_{\text{comp}} + \dot{I}_{\text{valve}} + \dot{I}_{\text{ORC,cond}} \tag{29}$$

The VCC system's exergy efficiency ($\eta_{\text{exergy,VCC}}$) may be defined as exergy extracted from the chilled water divided by compressor work. Hence, the efficiency is expressed as:

$$\eta_{exergy,VCC} = \frac{\dot{m}_{VCC}[h_5 - h_1 - T_0(s_5 - s_1)] - \dot{I}_{evap}}{\dot{W}_{comp}} \quad (30)$$

Similarly, the exergy efficiency ($\eta_{exergy,ORC}$) of the ORC subsystem can be given by:

$$\eta_{exergy,ORC} = \frac{\dot{E}_{net}}{\dot{E}_{in}} = \frac{\dot{E}_{net}}{\dot{m}_{ORC}[h_2 - h_3 - T_0(s_2 - s_3)]} \quad (31)$$

By applying waste heat recovery, the exergy efficiency ($\eta_{exergy,\ system}$) of the i-VCC—ORC system can be represented as:

$$\eta_{exergy,system} = \frac{\dot{m}_{VCC}[h_5 - h_1 - T_0(s_5 - s_1)] - \dot{I}_{evap}}{\dot{W}_{comp} - \dot{E}_{net}} \quad (32)$$

4.2.3. Exergetic analysis for air-air cooled integrated VCC—ORC system

As mentioned, ambient air and indoor exhaust air cooled the VCC and ORC condensers, respectively. Therefore, the thermodynamic equations governing exergetic analysis for this system is mentioned below. The subscript '*da*' will distinguish the exergy analysis for air-air-cooled systems.

The exergy destruction rate ($\dot{I}_{evap,da}$) and exergy efficiency ($\eta_{evap,da}$) of the evaporator are shown as.

$$\dot{I}_{evap,da} = \dot{m}_{VCC,da}T_0(s_{1,da} - s_{5,da}) + \dot{m}_{CW,dw}T_0(s_{15,da} - s_{14,da}) \quad (33)$$

$$\eta_{evap,da} = \frac{\dot{m}_{CW,da}[h_{15,da} - h_{14,da} - T_0(s_{15,da} - s_{14,da})]}{\dot{m}_{VCC,da}[h_{5,da} - h_{1,da} - T_0(s_{5,da} - s_{1,da})]} \quad (34)$$

where T_0 is the dead state temperature, $\dot{m}_{CW}$ is the mass flow rate of chilled water in the VCC system.

The exergy destruction rate ($\dot{I}_{comp,da}$) and exergy efficiency ($\eta_{comp,da}$) of the compressor can be written as:

$$\dot{I}_{comp,da} = \dot{m}_{VCC,da}T_0(s_{2,da} - s_{1,da}) \quad (35)$$

$$\eta_{comp} = \frac{(\dot{W}_{comp} - \dot{I}_{comp,da})}{\dot{W}_{comp}} \quad (36)$$

The exergy destruction rate ($\dot{I}_{valv,da}$) in the valve can be represented as:

$$\dot{I}_{valv,da} = \dot{m}_{VCC,da}T_0(s_{5,da} - s_{4,da}) \quad (37)$$

In the SHX, the exergy destruction rate ($\dot{I}_{SHX,da}$) and its exergy efficiency ($\eta_{SHX,da}$) are given by:

$$\dot{I}_{SHX,da} = \dot{m}_{VCC,da}T_0(s_{3,da} - s_{2,da}) + \dot{m}_{ORC,da}T_0(s_{11,da} - s_{9,da}) \quad (38)$$

$$\eta_{SHX,da} = \frac{\dot{m}_{VCC,da}[h_{2,da} - h_{3,da} - T_0(s_{2,da} - s_{3,da})] - \dot{I}_{SHX,da}}{\dot{m}_{VCC,da}[h_{2,da} - h_{3,da} - T_0(s_{2,da} - s_{3,da})]} \quad (39)$$

The exergy destruction rate ($\dot{I}_{VCC,cond,da}$) and exergy efficiency ($\eta_{VCC,cond,da}$) of the VCC condenser can be expressed as:

$$\dot{I}_{VCC,cond,da} = \dot{m}_{VCC,da}T_0(s_{4,da} - s_{3,da}) + \dot{m}_{AA,da}T_0(s_{17,da} - s_{16,da}) \quad (40)$$

$$\eta_{VCC,cond,da} = \frac{\dot{m}_{VCC,da}[h_{3,da} - h_{4,da} - T_0(s_{3,da} - s_{4,da})] - \dot{I}_{VCC,cond,da}}{\dot{m}_{VCC,da}[h_{3,da} - h_{4,da} - T_0(s_{3,da} - s_{4,da})]} \quad (41)$$

where ($\dot{m}_{AA,da}$) is the mass flow rate of ambient air responsible for cooling the VCC condenser.

Through the expansion process in the expander, the irreversible destruction rate ($\dot{I}_{turb,da}$) and its exergy efficiency ($\eta_{turb,da}$) are shown as:

$$\dot{I}_{turb,da} = \dot{m}_{ORC,da}T_0(s_{9,da} - s_{8,da}) \quad (42)$$

$$\eta_{turb,da} = \frac{\dot{m}_{ORC,da}(h_{8,da} - h_{9,da})}{\dot{m}_{ORC,da}(h_{8,da} - h_{9,da}) + \dot{I}_{turb,da}} \quad (43)$$

The exergy destruction rate ($\dot{I}_{ORC,cond,da}$) and exergy efficiency ($\eta_{ORC,cond,da}$) of the ORC condenser can be expressed as:

$$\dot{I}_{ORC,cond,da} = \dot{m}_{ORC,da}T_0(s_{8,da} - s_{12,da}) + \dot{m}_{EA,da}T_0(s_{19,da} - s_{18,da}) \quad (44)$$

$$\eta_{ORC,cond,da} = \frac{\dot{m}_{ORC,da}[h_{12,da} - h_{8,da} - T_0(s_{12,da} - s_{8,da})] - \dot{I}_{VCC,cond,da}}{\dot{m}_{ORC,da}[h_{12,da} - h_{8,da} - T_0(s_{12,da} - s_{8,da})]} \quad (45)$$

where ($\dot{m}_{EA,da}$) is the mass flow rate of exhaust indoor air.

The exergy destruction rate ($\dot{I}_{pump,da}$) and exergy efficiency ($\eta_{pump,da}$) of the pump can be defined as:

$$\dot{I}_{pump,da} = \dot{m}_{ORC,da}T_0(s_{9,da} - s_{8,da}) \quad (46)$$

$$\eta_{pump,da} = \frac{\dot{m}_{ORC,da}(h_{9,da} - h_{8,da}) - \dot{I}_{pump,da}}{\dot{m}_{ORC,da}(h_{9,da} - h_{8,da})} \quad (47)$$

The total exergy destruction ($\dot{I}_{total,da}$) in the integrated VCC—ORC system is the sum of the exergy destruction in each component, which can be given by Eq. (77):

$$\dot{I}_{total,da} = \dot{I}_{SHX,da} + \dot{I}_{AC,cond,da} + \dot{I}_{turb,da} + \dot{I}_{pump,da} + \dot{I}_{evap,da} + \dot{I}_{comp,da} + \dot{I}_{valv,da} + \dot{I}_{ORC,cond,da}$$

The exergy efficiency ($\eta_{exergy,VCC,da}$) of the VCC system may be defined as exergy extracted from the return chilled water divided by inlet compressor work. Hence, the efficiency is expressed as:

$$\eta_{exergy,VCC,da} = \frac{\dot{m}_{VCC,da}[h_{5,da} - h_{1,da} - T_0(s_{5,da} - s_{1,da})] - \dot{I}_{evap,da}}{\dot{W}_{comp,da}} \quad (48)$$

Similarly, the exergy efficiency ($\eta_{exergy,ORC,da}$) of the ORC subsystem can be given by:

$$\eta_{exergy,ORC,da} = \frac{\dot{E}_{net}}{\dot{E}_{in}} = \frac{\dot{E}_{net}}{\dot{m}_{ORC,da}[h_{2,da} - h_{3,da} - T_0(s_{2,da} - s_{3,da})]}$$

By applying waste heat recovery, the exergy efficiency ($\eta_{ex,comb,da}$) of the i-VCC—ORC system can be represented as:

$$\eta_{exergy,system,da} = \frac{\dot{m}_{VCC,da}[h_{5,da} - h_{1,da} - T_0(s_{5,da} - s_{1,da})] - \dot{I}_{evap,da}}{\dot{W}_{comp} - \dot{E}_{net}} \quad (49)$$

In the integrated system, the modeling of counter-flow heat exchangers is conducted using the Log Mean Temperature Difference (LMTD) method. To accurately represent the heat exchange process, the heat exchangers are divided into zones based on the different fluid phases involved, namely single-phase flow, boiling, and condensation [39]. The heat transfer coefficient (U_i) and the corresponding heat exchange area (A_i) are calculated within each zone. Considering the fluid's convective heat transfer resistances on both sides of the heat exchanger, the heat transfer coefficient (U_i) ensures a precise estimation of the heat transfer process.

$$\frac{1}{U_i} = \frac{1}{a_{i,hf}} + \frac{1}{a_{i,cf}} \quad (50)$$

The non-dimensional relationship developed by Chisholm and Wanniarachchi [40] is used to estimate the heat transfer coefficient of single-phase flow. The correlation for this estimation is expressed as follows:

$$Nu = 0.724\left(\frac{6\beta}{\pi}\right)^{0.646} Re^{0.583}Pr^{1/3} \quad (51)$$

where β is the chevron angle of the plates.

Table 6
Component cost in integrated VCC—ORC system using the desuperheating approach [43].

Component	Factor	Cost (€)
Pump	Required pump work, kW	$900\left(\frac{W_{pump}}{0.3}\right)^{0.25}$
Heat exchangers	Heat exchanger area, m2	$190+310(A)$
Expander	Volumetric flow rate, m3/s	$1.5(225+170.V_{turb})$
Compressor	Volumetric flow rate, m3/s	$225+170.V_{compressor})$
Refrigerant	Mass, kg	$20(M)$

The boiling process utilizes the Hsieh and Lin correlations [41], for the estimation. These correlations are expressed as follows:

$$a_{r,boiling} = a_{r,l}\left(0.88Bo^{0.5}\right) \tag{52}$$

$$a_{r,l} = 0.2092\left(\frac{k_l}{D_h}\right)Re^{0.78}Pr^{1/3}\left(\frac{\mu_m}{\mu_{wall}}\right)^{0.14} \tag{53}$$

$$Bo = \frac{q}{Gi_{fg}} \tag{54}$$

where $a_{r,l}$ is the all-liquid non-boiling heat transfer coefficient, and B_o is the boiling number.

Han, Lee, and Kim correlations are used to study the heat transfer coefficient of the condensation process [42]:

$$Nu = Ge_1 Re_{eq}^{Ge_2} Pr^{1/3} \tag{55}$$

$$Ge_1 = 11.2\left(\frac{p_{co}}{D_h}\right)^{-2.8}\left(\frac{\pi}{2}-\beta\right)^{-4.5} \tag{56}$$

$$Ge_2 = 0.35\left(\frac{p_{co}}{D_h}\right)^{0.2}\left(\frac{\pi}{2}-\beta\right)^{1.5} \tag{57}$$

$$Re_{eq} = \frac{G_{eq}D_h}{\mu_f} \tag{58}$$

$$G_{eq} = Ge\left[1-x+x\left(\frac{\rho_f}{\rho_v}\right)^{0.5}\right] \tag{59}$$

where Ge_1 and Ge_2 are non-dimensional geometric functions of the heat exchanger; Re_{eq} is the equivalent Reynolds number; G_{eq} is the equivalent mass flux; and P_{co} is the heat exchanger pinch; x is the quality of the refrigerant.

The U_i value and A_i can be determined for each zone within a single heat exchanger. The total heat exchange area (A) is obtained by summing up the A_i values from each zone, as expressed by the following equation:

$$A = \sum_{1}^{i} A_i \tag{60}$$

Thermo-economic analysis of the integrated VCC—ORC is conducted using the correlations used in Table 6 to estimate the cost of the components in the whole system. Moreover, the payback period is calculated by using the equation:

$$Payback_{yrs} = \frac{Total\ cost}{Electricity\ fee\ (€)\times\ 365days\times\ 24hrs\times\ E_{net}} \tag{61}$$

5. Results and discussion

5.1. Water-water cooled i-VCC—ORC system using desuperheating method

Table 7 presents the energetic and exergetic performances of five refrigerants in the VCC system combined with six different working fluids in the ORC system. The analysis focuses on key performance indices, including system COP, thermal efficiency, and exergy efficiency of the integrated system. Using simulation results obtained from EES, the R407c-R141b working pair demonstrates the highest performance in the water-water-cooled integrated VCC—ORC system.

It achieves a system COP of 3.20, thermal efficiency of 7.56 %, and net electricity output of 0.28 kW. The effects of ORC condensing water temperature, mass flow rate, and chilled water temperature on various

Table 7
Energy and exergy analysis for water-water cooled integrated system.

VCC Working fluid	ORC Working Fluid	COP_{VCC}	COP_{system}	$\dot{E}_{net}$ (kW)	ESR (%)	Payback period (yrs)	$\eta_{th,ORC}$ (%)	$\eta_{exergy,ORC}$ (%)	$\eta_{exergy,VCC}$ (%)	Integrated System	
										$\eta_{exergy,system}$ (%)	$\dot{I}_{total}$ (kW)
R134a	Butane	2.69	2.73	0.20	1.56	8.34	7.16	58.64	14.93	15.17	9.93
	R141b	2.69	2.73	0.21	1.62	11.81	7.41	60.65	14.93	15.18	9.92
	R227ea	2.69	2.73	0.19	1.43	7.78	6.57	53.81	14.93	15.15	9.94
	R245fa	2.69	2.73	0.20	1.56	10.44	7.17	58.75	14.93	15.17	9.93
	R1233zd(e)	2.69	2.73	0.21	1.58	10.68	7.24	59.26	14.93	15.17	9.93
R290	Butane	2.61	2.65	0.21	1.56	8.03	7.05	58.62	14.49	14.71	10.29
	R141b	2.61	2.65	0.22	1.61	11.44	7.29	60.6	14.49	14.72	10.28
	R227ea	2.61	2.65	0.19	1.43	7.44	6.48	53.87	14.49	14.70	10.30
	R245fa	2.61	2.65	0.21	1.56	10.06	7.07	58.74	14.49	14.71	10.29
	R1233zd(e)	2.61	2.65	0.21	1.57	10.31	7.13	59.23	14.49	14.72	10.29
R404A	Butane	2.31	2.35	0.28	1.86	7.93	6.46	56.42	12.83	13.07	11.94
	R141b	2.31	2.36	0.29	1.91	10.89	6.66	58.14	12.83	13.08	11.93
	R227ea	2.31	2.35	0.26	1.72	7.51	5.98	52.22	12.83	13.05	11.96
	R245fa	2.31	2.35	0.28	1.86	9.69	6.47	56.52	12.83	13.07	11.94
	R1233zd(e)	2.31	2.35	0.28	1.88	9.92	6.52	56.95	12.83	13.07	11.94
R407C	Butane	3.12	3.20	0.27	2.38	4.41	7.30	56.41	17.34	17.76	8.10
	R141b	3.12	3.20	0.28	2.46	5.03	7.56	58.40	17.39	17.83	8.09
	R227ea	3.12	3.20	0.25	2.18	4.73	6.69	51.66	17.34	17.73	8.12
	R245fa	3.12	3.20	0.27	2.39	4.90	7.32	56.53	17.34	17.77	8.10
	R1233zd(e)	3.12	3.20	0.27	2.41	4.92	7.38	57.03	17.34	17.77	8.10
R410A	Butane	2.75	2.84	0.41	3.20	6.37	7.38	53.34	15.27	15.77	9.46
	R141b	2.75	2.84	0.42	3.31	8.60	7.64	55.23	15.27	15.79	9.45
	R227ea	2.75	2.84	0.37	2.93	6.14	6.75	48.77	15.27	15.73	9.50
	R245fa	2.75	2.84	0.41	3.21	7.70	7.39	53.46	15.27	15.78	9.46
	R1233zd(e)	2.75	2.84	0.41	3.24	7.87	7.46	53.93	15.27	15.78	9.46

Table 8
Properties at various states for the R407c-R141b for water-water cooled integrated VCC—ORC system.

State no.	Fluid	Temperature (°C)	Pressure (MPa)	Enthalpy (kJ/kg)	Entropy (kJ/kg.K)
1	R407c	6.020	0.566	412.3	1.769
2	R407c	75.35	2.075	457.2	1.808
3	R407c	63.56	2.075	442.5	1.766
4	R407c	47.17	2.075	272.1	1.239
5	R407c	1.960	0.566	272.1	1.261
8	R141b	26.09	0.082	68.76	0.258
9	R141b	26.27	0.266	68.96	0.259
11	R141b	62.68	0.266	320.1	1.014
12	R141b	32.32	0.082	299.9	1.031
14	water	12.00	0.101	50.46	0.180
15	water	7.074	0.101	29.82	0.107
16	water	30.00	0.101	125.8	0.437
17	water	32.55	0.101	136.4	0.472
18	water	20.00	0.101	298.6	5.696
19	water	25.94	0.101	299.5	5.699

performance parameters such as system COP, COP_{VCC}, ORC thermal efficiency, net electricity output, system exergy efficiency, and system exergy destruction are thoroughly discussed. Additionally, Table 8 provides thermodynamic values at different state points for the water-water-cooled integrated VCC—ORC system under the specified design conditions mentioned in Table 2.

5.1.1. *Effect of ORC condensing water temperature*

This section will discuss the effect of ORC condensing water temperature on integrated VCC—ORC systems. The variation in COP_{VCC}, system COP, net electricity output, ORC thermal efficiency, system exergy efficiency, and system exergy destruction with changing ORC condensing water temperature has been analyzed, and the results are shown in Figs. 4–6. As the temperature of ORC condensing water is changed from 25 °C-35 °C, there is a net decrease in COP of the system and standalone COP of the VCC system, but an overall increase in system COP has been observed. The refrigeration capacity of the VCC system is fixed, along with the mass flow rate of the chilled water. The indoor air temperature is kept constant at 25 °C. So, as the temperature of the ORC

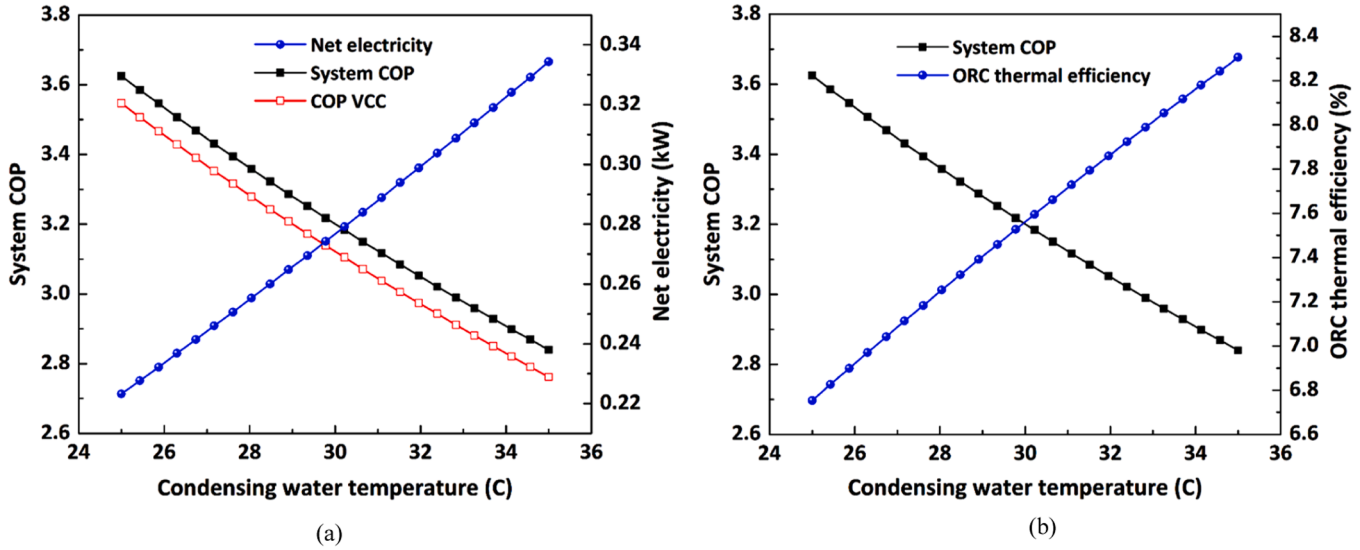

Fig. 4. Condensing water temperature vs. (a) System COP, COP_{VCC}, and Net electricity (b) System COP and ORC thermal efficiency.

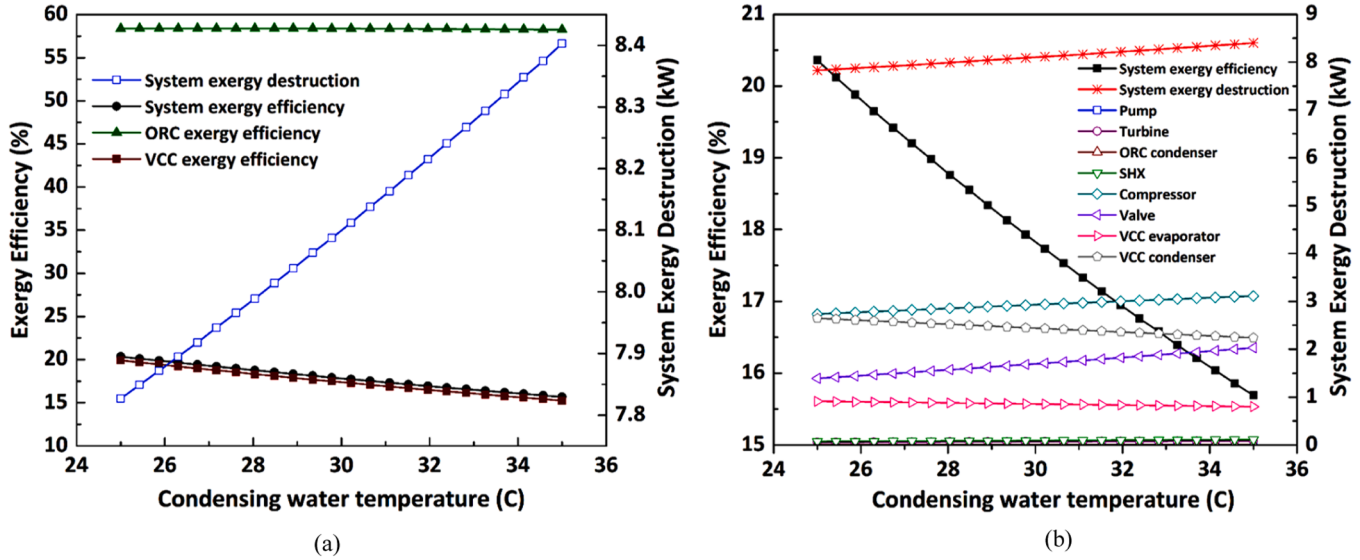

Fig. 5. Condensing water temperature vs.(a)System exergy efficiency and system exergy destruction (b) Components exergy efficiency and components exergy destruction.

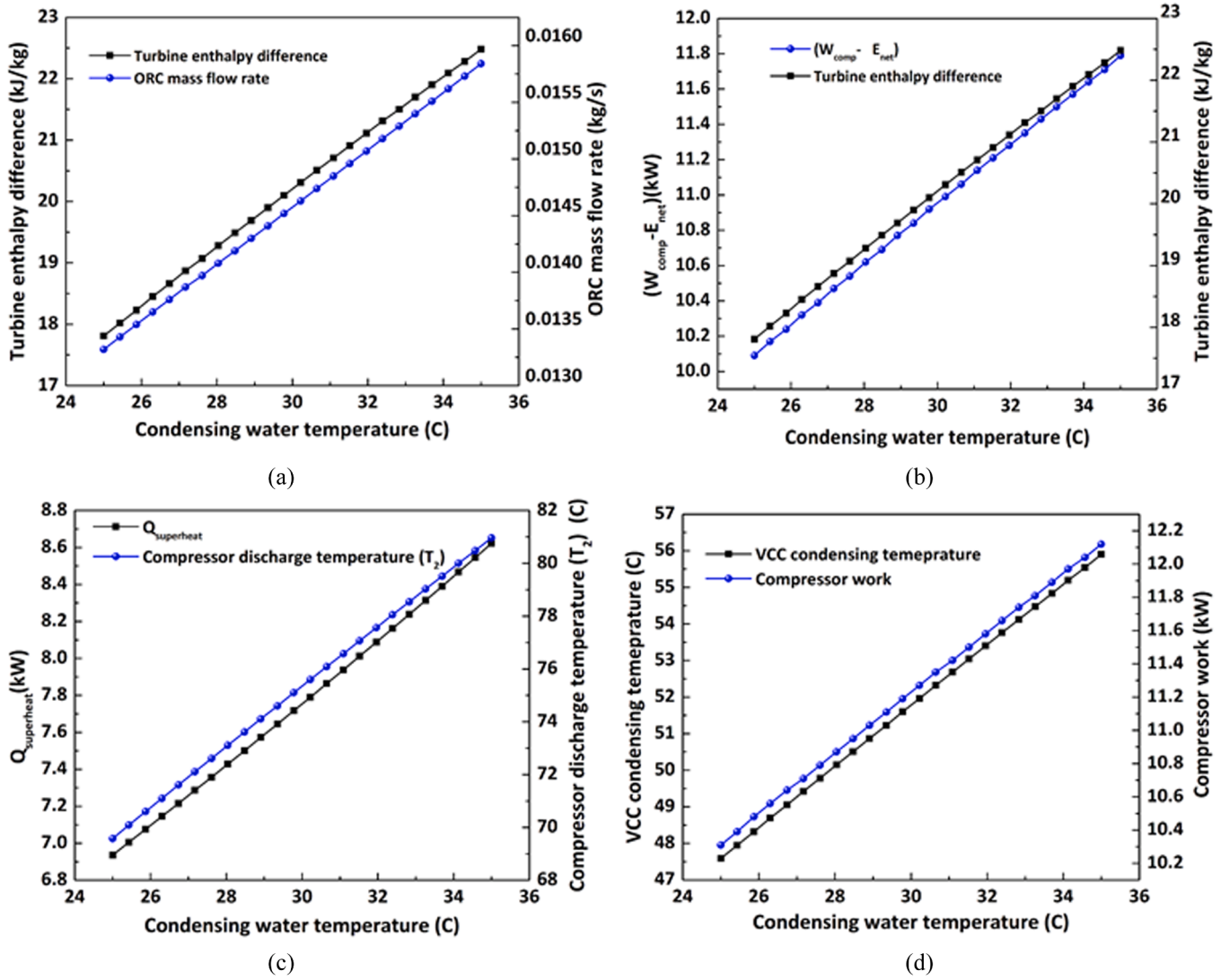

Fig. 6. Condensing water temperature vs.(a)Expander enthalpy difference and ORC mass flow rate (b)W_{comp}-E_{net} and Expander enthalpy difference (c)VCC condensing temperature and Compressor work (d)$Q_{superheat}$ and Compressor discharge temperature.

condensing water changes, the VCC condensing temperature and mass flow rate in the VCC start to increase with a corresponding increase in the VCC evaporation temperature. This increase increases net compressor work, as shown in Fig. 6(c). The result is a decrease in the standalone COP of the VCC system. With increasing ORC condensing air temperature, net electricity output and ORC thermal efficiency have also been observed. The increase in condensing water temperature increases the ORC condenser pressure, which increases the condenser temperature, resulting in a corresponding increase in ORC evaporator pressure. This increases the enthalpy difference across the ORC's expander and mass flow rate. As a result, the network output increases. As the system COP is dependent on the difference between the net electricity output and compressor work ($\dot{W}_{comp} - \dot{E}_{net}$), so with increasing values of both these factors, their difference also increases as shown in Fig. 5(b) resulting in net decrease in the overall system COP. Within the varied condensing water temperature from 20 °C-35 °C, the COP of the standalone VCC system and system COP decreases from 3.507 to 2.768 and 3.585 to 2.84 as compressor work and ($\dot{W}_{comp} - \dot{E}_{net}$) increases from 10.39 kW to 12.12 kW and 10.17 kW to 11.79 kW. The ORC thermal efficiency and net electricity increase from 6.83 % to 8.31 % and 0.23 kW to 0.33 kW within the varied range of ORC condensing water temperature. The values of COP_{VCC}, system COP, ORC thermal efficiency, and net electricity output are 3.122, 3.201, 7.56 %, and 0.28 kW at a condensing water temperature of 30 °C.

For exergetic analysis, there is a net decrease in system exergy efficiency and VCC exergy efficiency, whereas a slight decline in ORC exergy efficiency is also observed. Moreover, the system's exergy destruction increases as the condensing water temperature increases from 25 °C to 35 °C. As shown in the above equations, the exergy efficiencies are a function of mass flow rates in the ORC and VCC system, as well as the corresponding compressor work and net electricity output. With increased condensing air temperature, ORC condenser and evaporator temperature also increases. The corresponding VCC condensing temperature also rises to accommodate this increase, resulting in a net increase in the compressor work. Due to this increase in the compressor work, the overall exergy efficiency of the VCC system decreases. Although the exergy destruction is affected by the mass flow rate of refrigerant in VCC as well, the increase in the mass flow rate is minimal as compared to the increase in compressor work, which dominated the decreasing trend of the VCC exergy efficiency, as shown in Fig. 5(a). Similarly, the high-quality waste heat recovered from the superheated region of the VCC cycle increases the net electric work output. Still, the increase in the mass flow rate in the ORC system dominates more than the increase in the net electric work output. As a result, the ORC exergy efficiency declines. The system exergy efficiency is a function of

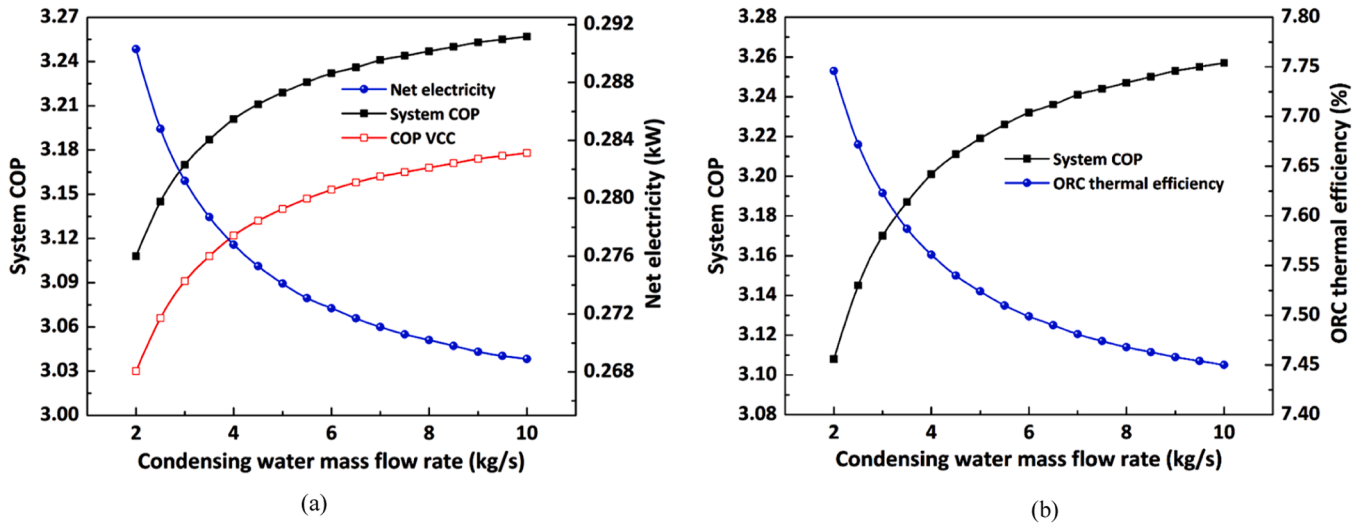

Fig. 7. Condensing water mass flow rate vs.(a)System COP, $COP_{VCC,}$ and Net electricity (b)System COP and ORC thermal efficiency.

$(\dot{W}_{comp} - \dot{E}_{net})$ which increases with the increasing condensing water temperature, resulting in a net decrease in system exergy efficiency. The VCC, ORC and system exergy values decrease from 19.92 % to 15.25 %, 58.39 % to 58.26 % and 20.36 % to 15.69 % as the $(\dot{W}_{comp}, \dot{E}_{net})$ and $(\dot{W}_{comp} - \dot{E}_{net})$ varies from 10.47 kW to 12.12 kW, 0.22 kW to 0.33 kW, and 10.09 kW to 11.79 kW. At 30 °C condensing air temperature, these parameters show values of 17.39 %, 58.39 %, and 17.83 %, respectively. Fig. 5(a) shows the variation of VCC, ORC, and system exergy efficiency with condensing water temperature.

With an increase in the mass flow rate of the condensing water, the exergy destruction in the integrated VCC—ORC system also increases. The mass flow rate of the condensing water, the temperature of the chilled water and the indoor air temperature play crucial roles in controlling the condensing and evaporating temperatures within the VCC cycle. At indoor air temperature and chilled water mass flow rate of 12 °C and 1.7 kg/s, the evaporation temperature of VCC is 2 °C, whereas the compressor discharge temperature is 75 °C. Whereas the ORC evaporation temperature is 63 °C.

As the condensing water temperature increases, the increase in the ORC condenser temperature results in a net increase in mass flow rate and the entropy difference across the ORC condenser. This increases the exergy destruction across the ORC condenser as the condensing water temperature increases. Similar is the case with the SHX, pump, and expander. The contribution of exergy destruction for the VCC compressor and expansion valve in system exergy destruction is more prominent than the other components in the integrated VCC—ORC system. Their exergy destruction values increase with increasing condensing air temperature.

The exergy destruction values decrease from the VCC evaporator and VCC condenser (excluding the superheat part of the VCC condenser). The overall system exergy destruction increases from 7.827 kW to 8.403 kW with an increasing mass flow rate of ORC condensing water. The variation of system exergy destruction and exergy destruction in components of the integrated VCC—ORC system is shown in Fig. 5(b). At an ORC condensing water temperature of 30 °C, the VCC—ORC has a system exergy destruction value of 8.10 kW.

5.1.2. Effect of ORC condensing water mass flow rate on integrated VCC—ORC system

In the previous section, the effect of condensing water temperature on integrated VCC—ORC system performance has been discussed in detail. However, the variation of changing mass flow rate also affects the thermodynamic performance of the integrated VCC—ORC system. In

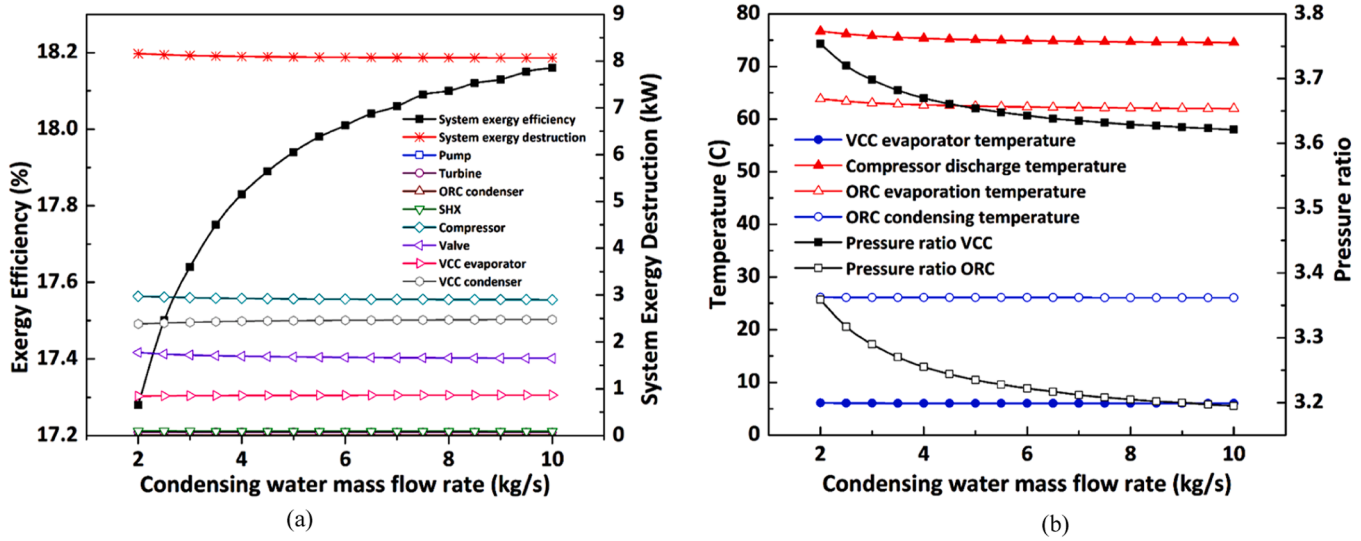

Fig. 8. Condensing water mass flow rate vs (a) System exergy efficiency and system exergy destruction (b) Temperature and Pressure ratio.

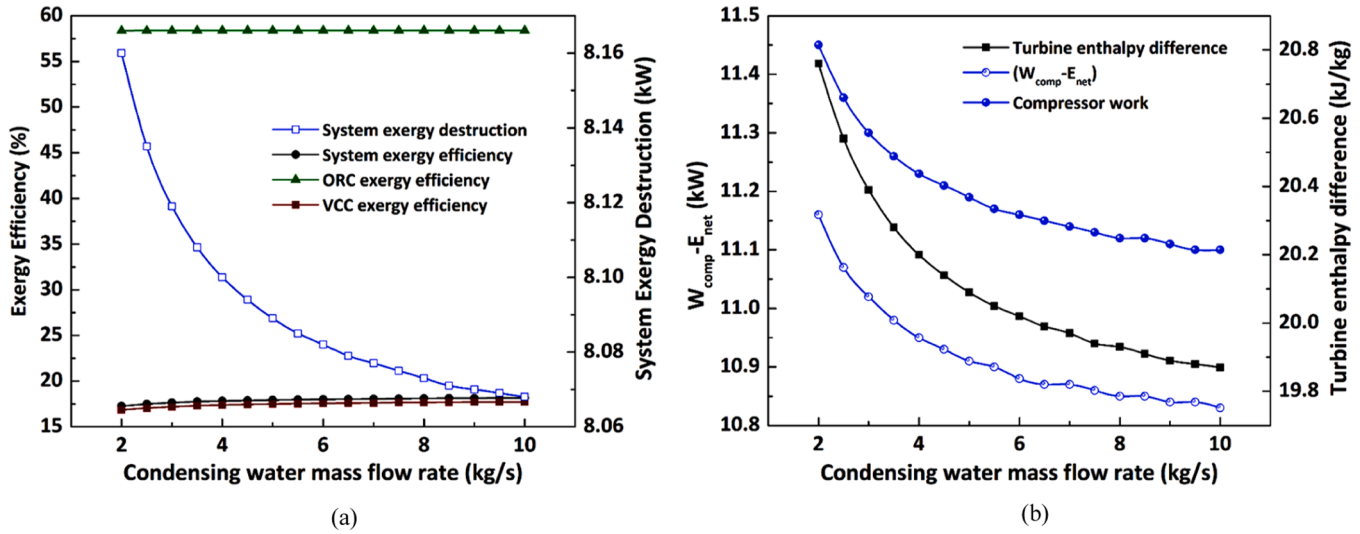

Fig. 9. Condensing water mass flow rate vs (a) Exergy efficiency and system exergy destruction (b) (W_{comp}-E_{net}) and enthalpy difference.

this section, the effect of ORC condensing water mass flow rate on integrated system COP, net electricity, ORC thermal efficiency, and exergetic performance will be discussed and shown in Figs. 7–9.

As the mass flow rate of ORC condensing air varies from 2 kg/s to 10 kg/s, the increase in the integrated system COP and standalone COP of the VCC system has been observed. However, there is a decrease in net electricity output and ORC thermal efficiency. At a fixed cooling capacity of the VCC system, the chilled water temperature and mass flow rate are also fixed at 12 °C and 1.7 kg/s to maintain the indoor air temperature of 25 °C. With these conditions, the mass flow rate of the refrigerant in the VCC system decreases very little (from 0.251 kg/s to 0.249 kg/s). As mentioned earlier, only the high-quality heat from the superheated region of VCC will be recovered, and the remaining heat will be discharged as ambient. Therefore, the VCC condenser, cooled by ambient water, also impacts the system's thermal performance. With the increasing mass flow rate of air on the ORC condenser side, the mass flow rate of the water in the VCC condenser (rejecting heat at ambient) will be increased from 3.45 kg/s to 3.51 kg/s. The result is a decrease in VCC evaporator and compressor discharge temperatures. The decline in compressor discharge temperature is more prominent than the decrease in VCC evaporation temperature. The net effect will be the decrease in the VCC pressure ratio, which ultimately decreases the compressor work and, hence, increases the COP of the VCC system. The variation in VCC pressure ratio, VCC evaporation temperature, compressor discharge temperature, and compressor work with changing ORC condensing water mass flow rate is shown in Fig. 9(a) and (b). The VCC pressure ratio, evaporation, and compressor discharge temperature reduce from 3.754 to 3.621, 6.08 °C to 5.99 °C and 76.71 °C to 74.54 °C as the condensing water mass flow rate is varied within the given range. Similarly, the increase in COP of the VCC is also represented in Fig. 7(a). At ORC condensing water mass flow rate of 4 kg/s, the COP of the VCC system is 3.122 whereas VCC pressure ratio, evaporation, and compressor discharge temperature values are 3.67, 6.02 °C and 75.35 °C respectively. A decrease in ORC thermal efficiency is also observed with the increase in the mass flow rate of condensing air. As the compressor outlet temperature decreases, the net heat available in the superheat region in the VCC cycle decreases, allowing less heat to be available to the ORC system. Also, due to the lower expander power output, the ratio of the net electric work output and the amount of superheat recovered from VCC decreases. The ORC thermal efficiency decreases from 7.75 % to 7.45 % as the condensing water mass flow rate increases. At 4 kg/s, the integrated VCC—ORC system shows a thermal efficiency of 7.56 %. The increase in integrated system COP depends on the difference between compressor work and net electricity output ($\dot{W}_{comp} - \dot{E}_{net}$). With the increase in the ORC condensing air mass flow rate, the ORC condensing temperature and pressure reduce condensing temperature and pressure reduce. Since the evaporation temperature of the ORC is not fixed, it is determined and governed by the conditions of the VCC cycle. So, as the ORC condensing water mass flow rate increases, the ORC refrigerant mass flow rate will reduce (from 0.0148 kg/s to 0.0144 kg/s) with a corresponding decrease in ORC evaporation and condensing temperature. This decreases the ORC pressure ratio, hence, the enthalpy difference across the expander also decreases. The decrease in the ORC evaporation temperature is more abrupt than the ORC condensing temperature, which declines very little. All these factors affect the decrease in net electricity output, as shown in Fig. 7(a).

As mentioned above, the compressor work decreases with increasing ORC condensing air mass flow rate. Hence, the net effect is the decreasing value of the factor ($\dot{W}_{comp} - \dot{E}_{net}$) due to which the system COP increases. The values of system COP increase from 3.108 to 3.257 as the factor ($\dot{W}_{comp} - \dot{E}_{net}$) decreases from 11.16 kW to 10.83 kW, as shown in Fig. 9(b). The system COP and ($\dot{W}_{comp} - \dot{E}_{net}$) has values of 3.20 and 10.83 kW at a simulated condition of ORC condensing water mass flow rate of 4 kg/s.

Moreover, the ORC pressure ratio, evaporation and condensing temperature and net electricity values reduce from 3.36 to 3.195, 63.83 °C to 61.99 °C, 26.12 °C to 26.07 °C and 0.290 kW to 0.269 kW. At ORC condensing water mass flow rate of 4 kg/s, 0.28 kW of net electricity is generated. In contrast, the values of ORC pressure ratio, evaporation and condensing temperature and enthalpy difference across the expander are 3.26, 62.68 °C, 26.09 °C and 20.2 kJ/kg, respectively. The variation of ORC pressure ratio, ORC evaporation and condenser temperatures with changing ORC condensing water mass flow rate is represented in Fig. 9(a), whereas the enthalpy difference variation is represented in Fig. 9(b).

The exergetic performance of the integrated VCC—ORC system with changing ORC condensing water mass flow rate is shown in Fig. 8(a) and (b). The system exergy efficiency, VCC and ORC exergy efficiency and system exergy destruction along with exergy destruction in components are also plotted against the ORC condensing air mass flow rate. The exergy efficiencies depend on compressor work, net electricity and mass flow rates in ORC and VCC. For VCC exergy efficiency, the VCC refrigerant mass flow rate almost remains the same (~0.25 kg/s). However, the VCC exergy efficiency rises due to decreased compressor work. The VCC exergy efficiency increases from 16.84 % to 17.72 % as compressor work varies from 11.45 kW to 11.10 kW. Similarly, ORC exergy

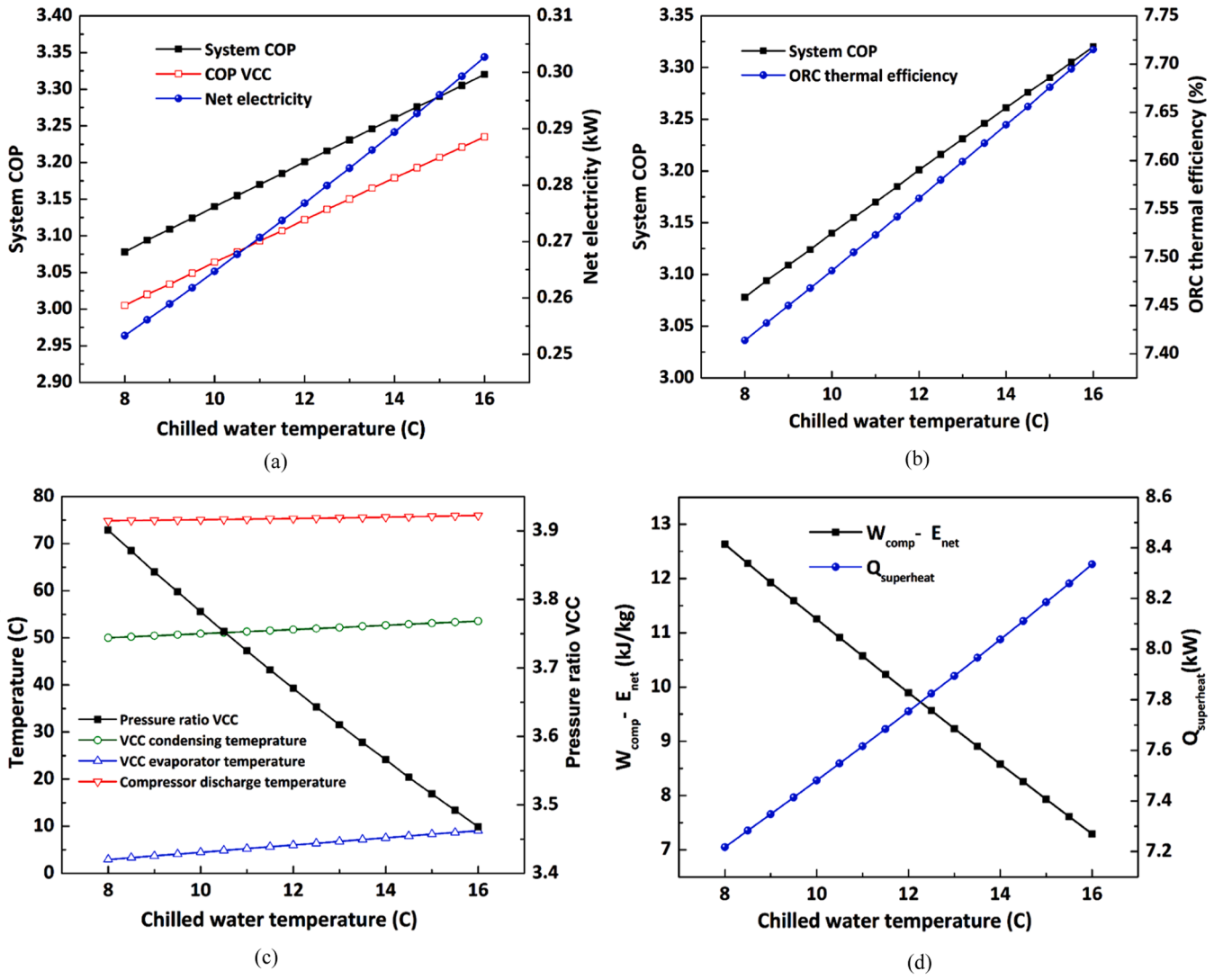

Fig. 10. Chilled water temperature vs.(a)System COP, $COP_{VCC,}$ and Net electricity (b)System COP and ORC thermal efficiency (c)VCC cycle temperatures and pressure ratio (d) (W_{comp}-E_{net}) and $Q_{superheat}$.

efficiency almost remains the same (~58.40 %) with varying ORC condensing air mass flow rates. This is because as the enthalpy difference across the expander decreases, net electricity output decreases, but the ORC mass flow rate decreases in such a way that the ORC exergy efficiency almost remains the same throughout. Similarly, the system exergy efficiency increases with a decrease in the difference between compressor work and net electricity value ($\dot{W}_{comp} - \dot{E}_{net}$). The compressor work and net electricity values decrease, and so does the factor ($\dot{W}_{comp} - \dot{E}_{net}$), resulting in a net increase in the system exergy efficiency. The system exergy efficiency increases from17.28 % to 18.16 % as ($\dot{W}_{comp} - \dot{E}_{net}$) decreases from 11.16 kW to 10.83 kW as shown in Fig. 8(a) and 9(b). At 4 kg/s, the VCC, ORC, and system exergy values are 17.39 %, 58.40 %, and 17.83 %, respectively. With an increase in the ORC condensing water temperature, the total exergy destruction of the integrated VCC—ORC system exhibits a decreasing trend, reducing from 8.16 kW at 2 kg/s to 8.07 kW at 10 kg/s. However, when analysing the individual components of the integrated VCC—ORC system, it is observed that some components experience an increasing trend in exergy destruction while others demonstrate a decreasing trend. In the VCC system, the valve and compressor show a decreasing exergy destruction trend, whereas in the ORC system, the exergy destruction in the pump, expander, and ORC condenser decreases. The exergy destruction rate increases in the VCC condenser (rejecting heat at ambient) and evaporator. The condensing water temperature in the VCC is kept at ambient (30 °C). So, as the mass flow rate of the ORC condensing air increases, the water in the VCC condenser also increases to cool down the refrigerant coming from the SHX. With reducing compressor discharge temperature, the temperature of the water exiting from the VCC condenser also decreases. Since the mass flow rate in the VCC almost remains the same, the terminal temperature difference rises, reducing the capability of the VCC condenser to transfer the heat, which increases the net exergy destruction rate in the VCC condenser. Similar is the case in the VCC evaporator.

The chilled water temperature and mass flow rate are kept constant. The increasing temperature difference value in the evaporator on the water and refrigerant sides increases the VCC evaporator's exergy difference. The overall effect is a decreased system exergy destruction value, as shown in Fig. 8(a) and (b).

5.1.3. Effect of chilled water temperature on integrated VCC—ORC system

The chilled water in the evaporator governs the VCC evaporation and condensing temperature. The effect of changing chilled water temperature on the thermodynamic performance of water-cooled VCC and air-cooled ORC integrated systems will be discussed in this section. The chilled water temperature in the VCC evaporator varies from 8 kg/s to

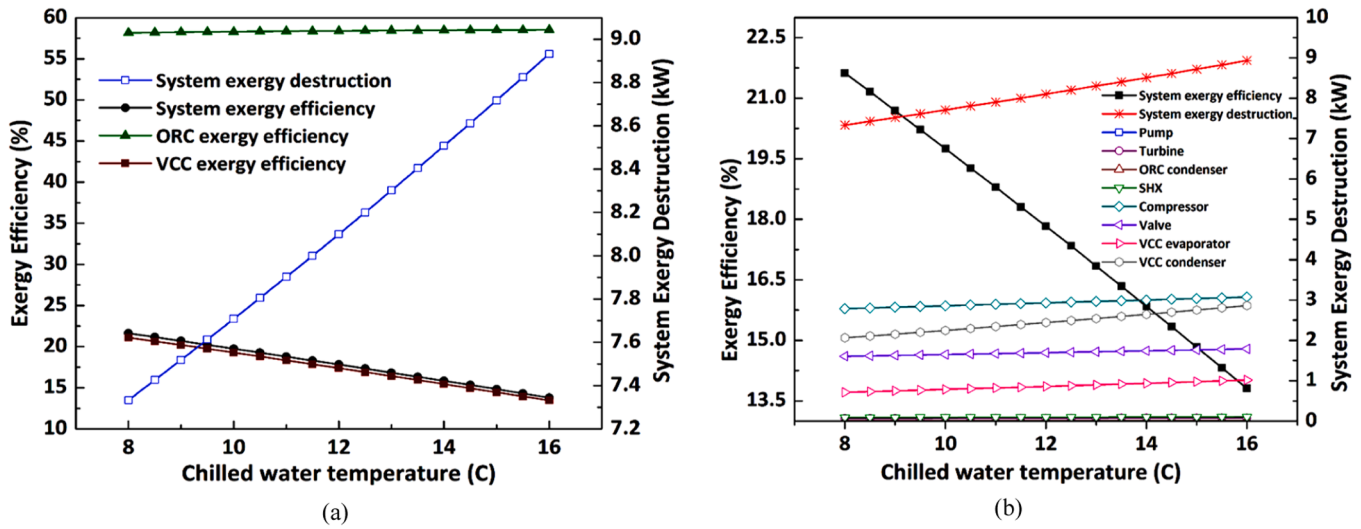

Fig. 11. Chilled water temperature vs.(a) System exergy efficiency and System exergy destruction (b) Components exergy efficiency and components exergy destruction.

16 kg/s, and the mass flow rate is kept constant at 1.7 kg/s. The indoor air temperature is also maintained at 25 °C. At these conditions, when the chilled water temperature increases, the VCC evaporator and condensing temperature also increase. The increase in the VCC evaporation temperature is more prominent than the relative decrease in the VCC condensing temperature. The overall result is a decrease in the VCC pressure ratio. As the pressure ratio of the VCC system decreases, the compressor work also decreases, and the standalone COP of the VCC system increases, as shown in Fig. 9(a). the COP of the VCC system increases from 3.01 to 3.24 as the enthalpy difference across the compressor decreases from 47.18 kJ/kg to 42.75 kJ/kg. At a chilled water temperature of 12 °C, the COP of the VCC system is 3.12 at a compressor enthalpy difference value of 44.89 kJ/kg. However, with increasing chilled water temperature, the compressor discharge temperature shows an increasing trend, and therefore, the difference between the compressor discharge temperature and saturated vapor temperature at the VCC condenser inlet increases, resulting in a net increase in the amount of superheat (temperature difference between T_2 and T_3). The overall variation of VCC cycle temperatures and pressure ratio is shown in Fig. 10(c). The increment in temperature difference between the compressor discharge temperature and saturated vapour temperature at the VCC condenser inlet increases the value of $Q_{superheat}$. The system's COP, net electricity, and ORC thermal efficiency increase as the temperature of the chilled water increases. The decrease in the enthalpy difference across the compressor and increase in the enthalpy difference across the expander results in the net decrease in the factor $(\dot{W}_{comp} - \dot{E}_{net})$, and therefore, the system COP increases. On the other hand, the ORC condensing temperature almost remains the same (26 °C), and the values for mass flow rate and ORC condensing water temperature also remain the same at 4 kg/s and 30 °C. So, as the chilled

Table 9
Energy and exergy analysis for an air-air-cooled integrated system.

VCC Working fluid	ORC Working Fluid	COP_{ini}	COP_{comb}	$\dot{E}_{net}$ (kW)	ESR (%)	Payback period (yrs)	$\eta_{th.ORC}$ (%)	$\eta_{ex.ORC}$ (%)	$\eta_{ex.AC}$ (%)	Integrated System	
										η_{ex} (%)	$\dot{I}_{total.d}$ (kW)
R134a	Butane	2.76	2.80	0.19	1.53	8.51	7.02	58.73	15.31	15.54	8.40
	R141b	2.76	2.80	0.20	1.58	12.06	7.26	60.70	15.31	15.55	8.40
	R227ea	2.76	2.80	0.18	1.41	7.93	6.45	54.00	15.31	15.53	8.42
	R245fa	2.76	2.80	0.20	1.53	10.65	7.03	58.84	15.31	15.55	8.40
	R1233zd(e)	2.76	2.80	0.20	1.54	10.91	7.09	59.33	15.31	15.55	8.40
R290	Butane	2.68	2.72	0.20	1.52	8.20	6.91	58.73	14.88	15.11	8.71
	R141b	2.68	2.72	0.21	1.57	11.69	7.14	60.67	14.88	15.12	8.70
	R227ea	2.68	2.72	0.18	1.40	7.58	6.36	54.07	14.88	15.09	8.72
	R245fa	2.68	2.72	0.19	1.52	10.28	6.92	58.84	14.88	15.11	8.71
	R1233zd(e)	2.68	2.72	0.20	1.54	10.54	6.98	59.32	14.88	15.11	8.71
R404A	Butane	2.36	2.41	0.27	1.82	8.04	6.37	56.56	13.12	13.36	10.38
	R141b	2.36	2.41	0.28	1.88	11.06	6.56	58.26	13.12	13.37	10.37
	R227ea	2.36	2.40	0.25	1.69	6.82	6.59	52.41	13.12	13.34	10.40
	R245fa	2.36	2.41	0.27	1.82	9.84	6.38	56.66	13.12	13.36	10.38
	R1233zd(e)	2.36	2.41	0.27	1.84	10.07	6.43	57.08	13.12	13.36	10.38
R407C	Butane	3.15	3.23	0.26	2.36	4.45	7.25	56.45	17.52	17.94	6.86
	R141b	3.15	3.23	0.27	2.44	5.08	7.50	58.42	17.52	17.95	6.85
	R227ea	3.15	3.22	0.24	2.16	4.76	6.65	51.74	17.52	17.90	6.88
	R245fa	3.15	3.23	0.26	2.37	4.94	7.27	56.57	17.52	17.94	6.86
	R1233zd(e)	3.15	3.23	0.27	2.39	4.96	7.33	57.06	17.52	17.94	6.86
R410A	Butane	2.73	2.82	0.41	3.22	6.34	7.41	53.31	15.17	15.67	8.42
	R141b	2.73	2.83	0.44	3.33	8.56	7.67	55.21	15.17	15.69	8.41
	R227ea	2.73	2.81	0.38	2.94	6.13	6.77	48.72	15.17	15.63	8.45
	R245fa	2.73	2.82	0.41	3.22	7.66	7.43	53.43	15.17	15.67	8.42
	R1233zd(e)	2.73	2.82	0.42	3.25	7.83	7.49	53.90	15.17	15.68	8.42

Table 10
The properties at various states for the R410a-R141b desuperheating air-air cooled VCC—ORC system.

State no.	Fluid	Temperature (°C)	Pressure (MPa)	Enthalpy (kJ/kg)	Entropy (kJ/kg K)
1	R410a	2.030	0.851	422.0	1.807
2	R410a	81.15	3.062	471.9	1.850
3	R410a	65.57	3.062	450.2	1.787
4	R410a	49.87	3.062	285.6	1.279
5	R410a	1.965	0.851	285.6	1.311
8	R141b	26.65	0.083	69.40	0.261
9	R141b	26.84	0.276	69.62	0.261
11	R141b	64.00	0.276	321.0	1.014
12	R141b	33.11	0.083	300.5	1.031
14	water	12.00	0.101	50.46	0.180
15	water	7.077	0.101	29.84	0.108
16	air	35.00	0.101	308.6	5.729
17	air	45.52	0.101	319.2	5.763
18	air	20.00	0.101	298.6	5.696
19	air	26.43	0.101	300.0	5.700

water temperature increases, the compressor discharge temperature increases, and at a constant pinch temperature, the ORC evaporator temperature also increases. This increases the mass flow rate and enthalpy difference across the expander, and as a result, the net electricity output of the system increases. The net electricity value increases from 0.253 kW to 0.303 kW as the mass flow rate in ORC and enthalpy difference across the expander increases from 0.014 kg/s to 0.016 kg/s and 19.76 kJ/kg to 20.67 kJ/kg. Similarly, the value of $Q_{superheat}$ also increases as the chilled water temperature increases, increasing the net heat available across the SHX to the ORC system. So, with increasing value of $Q_{superheat}$ and net electricity output, the ORC thermal efficiency also increases, as shown in Fig. 10(d). The system COP and ORC thermal efficiency values increase from 3.08 to 3.32 and 7.41 % to 7.72 % as the chilled water temperature is increased from 8 °C to 16 °C. At 12 °C, the values of system COP and ORC thermal efficiency are 3.20 and 7.56 %, respectively. The increasing trend of system COP, net electricity output and ORC thermal efficiency is shown in Fig. 10(a) and (b).

The effect of chilled water temperature on system exergetic performance is also shown in Fig. 11. VCC, ORC, and system exergy efficiency with exergy destruction in the system and components of the integrated VCC—ORC system are also represented in Fig. 10(b). With increasing chilled water temperature, the VCC exergy efficiency will decrease, whereas the ORC exergy efficiency will increase slightly. However, there is a net decrease in the system's exergy efficiency. The reason mentioned earlier is that the system exergy efficiency depends on the difference

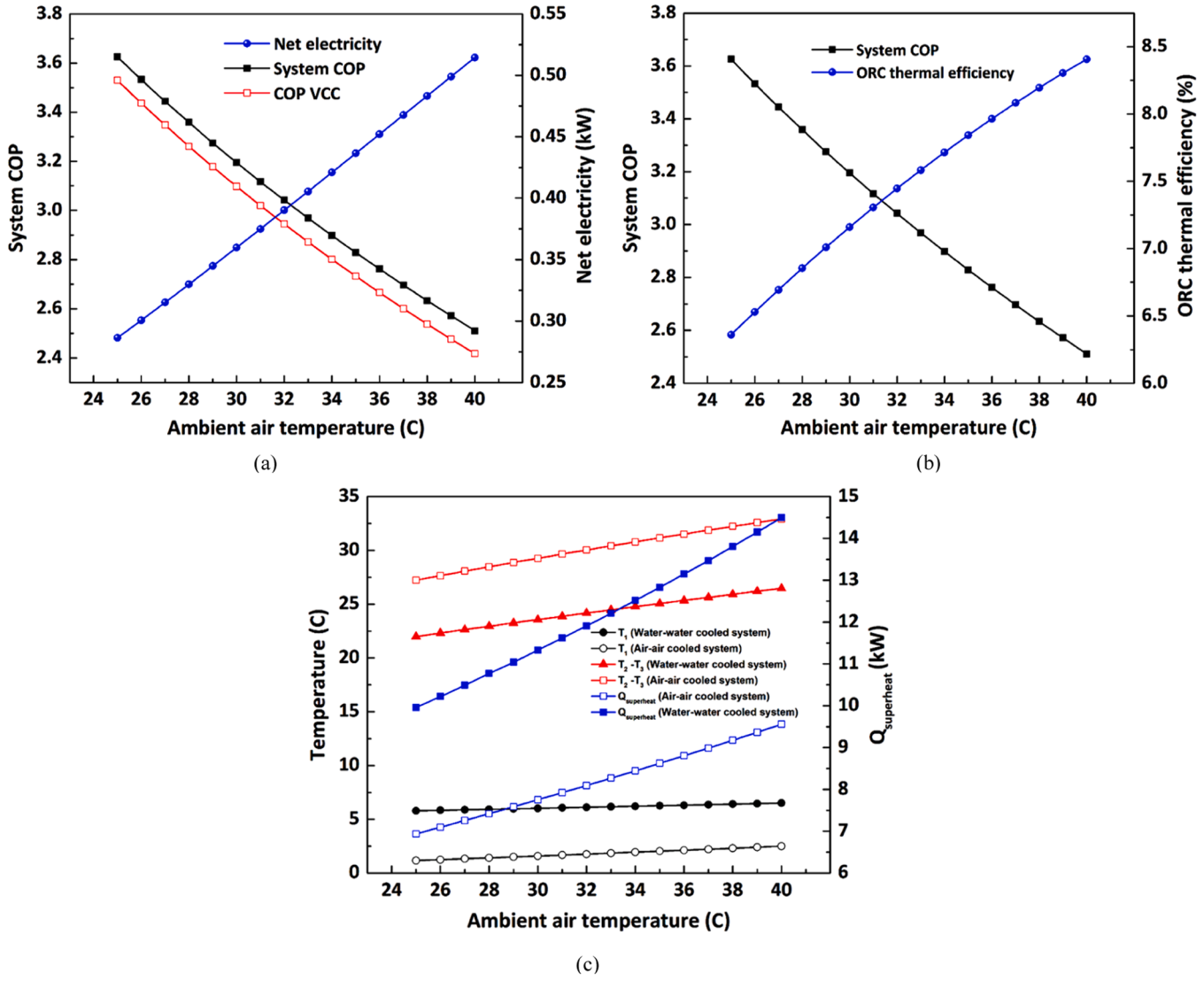

Fig. 12. Ambient air temperature vs.(a) System COP, COP_{VCC} and Net electricity (b) System COP and ORC thermal efficiency(c)T_1 and (T_2-T_3) for water-water and air-air cooled systems and $Q_{superheat}$.

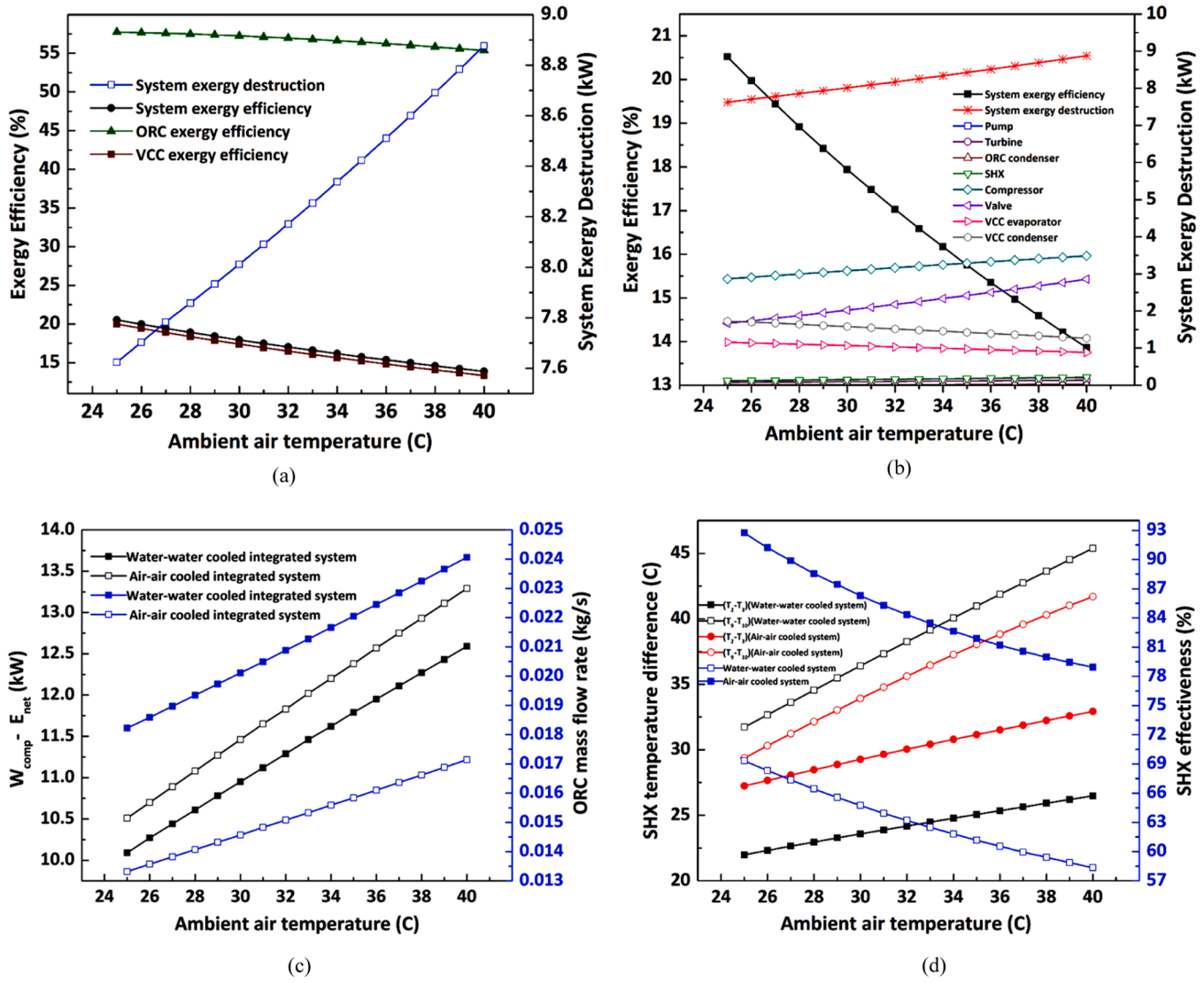

Fig. 13. Ambient air temperature vs (a) Exergy efficiency and System exergy destruction (b) Components exergy efficiency and Components exergy destruction(c) W_{comp}-E_{net} and ORC mass flow rate (d)SHX temperature difference and SHX effectiveness.

between ($\dot{W}_{comp} - \dot{E}_{net}$), which is further dependent on the enthalpy difference across the compressor and expander. So, as this factor increases, the system's exergy efficiency decreases. The VCC and system exergy efficiency decreases from 21.10 % to 13.46 % and 21.62 % to 13.81 %, whereas the ORC exergy efficiency increases from 58.17 % to 58.52 %. At a chilled water temperature of 12 °C, VCC, ORC, and system exergy efficiencies are 17.39 %, 58.40 %, and 17.83 %, respectively. Similarly, the system exergy destruction and the exergy destruction in components of the integrated VCC—ORC system are also shown in Fig. 11(b). The system exergy destruction rate increases from 7.33 kW to 8.93 kW. >50 % of the exergy destruction rate is contributed by the compressor and VCC condenser rejecting heat at ambient. This is because as the mass flow rate in the VCC increases, the temperature difference and heat transfer rate between the refrigerant and cooling media decreases, resulting in a net increase in the exergy destruction rate.

5.2. Air – air-cooled integrated VCC—ORC system

Table 9 shows the energetic and exergetic performance of the air-air-cooled integrated VCC—ORC system. Ambient air is used to cool the VCC condenser, whereas indoor exhaust air is used to cool the ORC condenser. From the perspective of net electricity and ORC thermal efficiency, R410a-R141b is chosen as the best pair, showing the maximum net electricity output (0.43 kW) and ORC thermal efficiency (7.67 %). The properties of this working fluid combination at various state points are also shown in Table 9. The effect of ORC condensing air temperature, mass flow rate, and indoor air temperature on system COP, COP_{VCC}, ORC thermal efficiency, net electricity output, system exergy efficiency, and system exergy destruction is discussed in detail (Table 10).

5.2.1. Effect of ambient air temperature

This section will discuss the effect of ambient air temperature on the integrated VCC—ORC system. The analysis investigates the impact of changing ambient air temperature on COP_{VCC}, system COP, net electricity output, ORC thermal efficiency, system exergy efficiency, and system exergy destruction. The results of this analysis are presented in Figs. 12 and 13. Comparing the trends between the water-water-cooled VCC—ORC system and the air-air-cooled VCC—ORC system, we observe that the variations in COP_{VCC}, system COP, net electricity output, system exergy efficiency, and system exergy destruction are similar. The ORC refrigerant remains the same, but the refrigerant in the VCC system is selected based on better ORC thermal efficiency and net electricity output as compared to the previous case in which R407c-R141b is

selected for analysis in a water-air cooled VCC—ORC system. With increasing ORC condensing (ambient) air temperature, the COP_{VCC} and system COP of the integrated system decreases with an increase in the net electricity output. The indoor air temperature, cooling capacity, and chilled water mass flow rate of the VCC cycle are kept constant. The increase in the ORC condensing (ambient) air temperature, the VCC condensing temperature, the evaporation temperature, and the mass flow rate of the refrigerant in VCC will be increased. The rise in the VCC condensing temperature is higher than the VCC evaporation temperature resulting in the VCC evaporation temperature, resulting in a net increase in the pressure ratio of the VCC system, resulting in a net increase in the compressor work. As a result, the COP of the standalone system declines. The VCC evaporation temperature increases from 1.16 °C to 2.51 °C whereas the VCC condensing temperature rises from 41.67 °C to 54 °C. The VCC system's pressure ratio and net compressor work also increase from 3.04 to 3.88 and 10.80 kW to 13.80 kW, resulting in a net decrease in the COP_{VCC} from 3.53 to 2.42. At 35 °C condensing (ambient) air temperature, the standalone COP of the VCC system is 2.73 at VCC evaporating and condensing temperatures of 2.03 °C and 50 °C. However, just for comparison with the water-water-cooled VCC—ORC system, when the ORC condensing water temperature is 20 °C, the COP of the VCC system is 3.55, which is slightly higher as compared to the air-air cooled VCC—ORC system. Similarly, the system COP, net electricity, and ORC thermal efficiency increase as the ORC condensing (ambient) air temperature increases. As the ORC condensing (ambient) air temperature increases, the condensing temperature of the ORC cycle rises with an increase in the ORC evaporation temperature. The net increment in the ORC evaporation temperature is higher than the ORC condensing temperature. As a result, the pressure ratio of the ORC system increases. The net increase in the pressure ratio increases the enthalpy difference across the expander, and hence, the net electricity output across the expander increases. The amount of $Q_{superheat}$ is higher in the air-air-cooled VCC—ORC system than in the water-water-cooled VCC—ORC system. The reason is that the air-air-cooled VCC—ORC system achieves low VCC evaporation and condensing temperatures. The VCC condenser is cooled by air. The mass flow rate depends on the temperature difference between ambient air and indoor air and the specific heat (C_p) value of air. So, for fixed cooling capacity and indoor air temperature, as the difference increases, the mass flow rate of the air decreases. Due to the higher mass flow rate of air at low ambient air temperature, the VCC condensing temperature for an air-air-cooled VCC—ORC system is less than the water-water-cooled VCC—ORC system.

Therefore, the temperature difference between compressor discharge temperature (T_2) and saturated vapour temperature at the VCC condenser (T_3) increases, thereby increasing the value of $Q_{superheat}$. The variation of VCC evaporation temperature (T_1) and the difference of compressor discharge temperature and VCC condensing temperature (T_2-T_3) for water-air and air-air cooled VCC—ORC system with ORC condensing (ambient) air temperature is shown in Fig. 12(c). The greater value of (T_2-T_3) and higher mass flow rate of the cooling air in the VCC condenser (rejecting heat at ambient) for air-air cooled VCC—ORC system results in the net increase in the value of $Q_{superheat,}$ which in turn increases the heat supply to the ORC system and hence the ORC thermal efficiency and net electricity output increases. The value of $Q_{superheat}$ for air-air cooled VCC—ORC system increases from 9.96 kW to 14.5 kW, whereas for water-air cooled VCC—ORC system, it increases from 6.94 kW to 9.56 kW as the ORC condensing (ambient) air temperature increases from 25 °C to 40 °C.

Similarly, the exergetic performance of the air-air-cooled VCC—ORC system is also shown in Fig. 12. As the ORC condensing (ambient) air temperature increases, the VCC, ORC, and system exergy efficiency decreases, as shown in Fig. 13(a). The decrease in the VCC exergy efficiency for an air-air-cooled VCC—ORC system is greater than that of the water-water-cooled integrated system within the varying temperature range of ORC condensing (ambient) air. The reason is that the increase in net compressor work for an air-air-cooled integrated system is greater as compared to the water-water-cooled integrated system. The VCC exergy efficiency for an air-air-cooled integrated system decreases from 19.98 % to 13.34 %, whereas compressor work increases from 10.80 kW to 13.80 kW for a water-water-cooled system. For a water-water-cooled integrated system, the VCC exergy value decreases from 19.92 % to 13.42 % as compressor work increases from 10.31 kW to 12.99 kW. Similarly, the ORC exergy value decreases with increasing ORC condensing (ambient) air temperature. The overall ORC exergy efficiency for a water-water-cooled integrated system is better than the air-air-cooled ORC system. The reason is the mass flow rate of the refrigerant in the ORC. The increase in the ORC mass flow rate for an air-air-cooled integrated system is greater than the water-water-cooled integrated system, due to which the decline in ORC exergy efficiency in the case of an air-air-cooled integrated system is greater. At 35 °C condensing (ambient) air temperature, air-air-cooled and water-water-cooled integrated systems show ORC exergy efficiencies of 56.44 % and 58.26 %, respectively. The ORC exergy efficiency decreases from 57.74 % to 55.36 % as the mass flow rate in the ORC increases from 0.0182 kg/s to 0.0241 kg/s, whereas for water-air cooled integrated system, the ORC exergy efficiency decreases from 58.39 % to 58.03 % as the mass flow rate in ORC increases from 0.0133 kg/s to 0.0171 kg/s. The exergy efficiency for both systems decreases as condensing (ambient) air temperature increases. The decrease in both cases is almost identical. Although the decrease in compressor work for the water-air cooled integrated system is less (10.31 kW-12.99 kW) as compared to the air-air cooled integrated system (10.80 kW-13.80 kW) but this is balanced by the increased amount of net electricity generated by the air-air-cooled-integrated-system (0.286 kW-0.515 kW) as compared to the water-air cooled integrated system (0.223 kW-0.396 kW).

The result is that the $(\dot{W}_{comp} - \dot{E}_{net})$ for an air-air-cooled integrated system is slightly more than the water-water-cooled integrated system, but a slightly higher mass flow rate in the VCC system for an air-air-cooled integrated system increases the overall system exergy efficiency. The system exergy efficiency for an air-air-cooled integrated system decreases from 20.52 % to 13.86 %, whereas for a water-water-cooled integrated system, it decreases from 20.36 % to 13.85 %. At 35 °C condensing (ambient) air temperature, air-air-cooled and water-water-cooled integrated systems show system exergy efficiencies of 15.75 % and 15.69 %. The variation of $(\dot{W}_{comp} - \dot{E}_{net})$ and ORC mass flow rate for air-air-cooled and water-water-cooled integrated systems is shown in Fig. 13(c).

The system's exergy destruction also increases with the increase in ORC condensing (ambient) air temperature. For the air-air-cooled integrated system, the increase in the system exergy destruction is higher than in the water-air integrated system. The reason is that the increase in the mass flow rates in the VCC and ORC systems for the air-air-cooled integrated system is greater than that of the water-air integrated system. This increases the terminal temperature difference across the SHX. Therefore, the heat transfer capability or heat recovery across SHX decreases, increasing the exergy destruction. The exergy destruction increases from 7.624 kW to 8.877 kW for an air-air-cooled integrated system, whereas, for a water-water-cooled system, it increases from 7.827 kW to 8.737 kW. For an air-air-cooled integrated system, the exergy destruction rate increases from 0.121 kW to 0.213 kW, whereas for a wat-air-cooled integrated system, it increases from 0.076 kW to 0.137 kW. In both cases, the effectiveness of SHX decreases, so the exergy destruction in the SHX increases.

5.2.2. *Effect of condensing air mass flow rate*

In the previous section, the effect of ambient air temperature on the performance of an integrated system has been analyzed. In this section, the ORC condensing air, which is the indoor exhaust air, has been selected as a performance indicator for analyzing the system's

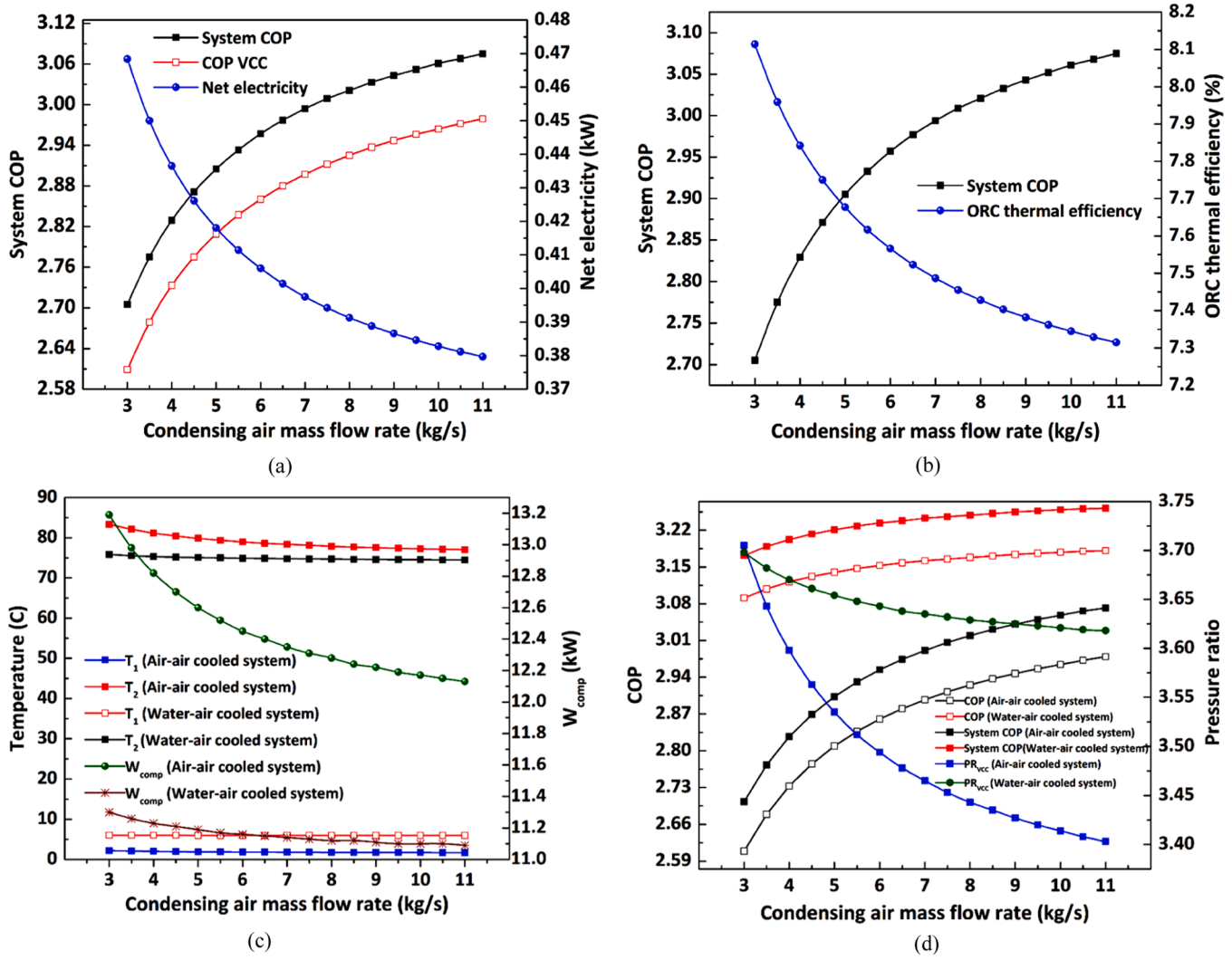

Fig. 14. Condensing air mass flow rate vs.(a)System COP, COP_{VCC} and Net electricity (b)System COP and ORC thermal efficiency(c)VCC Evaporation (T_1) and compressor discharge temperature(T_2) and W_{comp} (d)COP and PR_{VCC}.

thermodynamic response. The effect of changing ORC condensing (indoor exhaust) air mass flow rate will be discussed in this section. The performance of the air-air-cooled integrated VCC—ORC system will be compared to that of the water-water-cooled system. Fig. 14(a) and (b) depict the variation of COP_{VCC}, system COP, net electricity, and ORC thermal efficiency with varying ORC condensing water mass flow rates for the air-air-cooled VCC—ORC system. Comparing these results to Fig. 3(a) and (b) for the water-water-cooled VCC—ORC system, we observe a similar trend in the COP_{VCC}, system COP, net electricity, and ORC thermal efficiency for the air-air-cooled VCC—ORC system. However, the water-water-cooled system exhibits better COP_{VCC} and system COP than the air-air-cooled VCC—ORC system. In the case of the air-air-cooled VCC—ORC system, the COP_{VCC} increases from 2.61 to 2.98 as the ORC condensing air mass flow rate varies from 3 kg/s to 11 kg/s. Conversely, for the same range of variation in ORC condensing water mass flow rate in the water-water-cooled VCC—ORC system, the COP_{VCC} varies from 3.09 to 3.18. For system COP, the air-air-cooled system varies from 2.71 to 3.08, whereas the water-water-cooled system shows a system COP variation from 3.17 to 3.26. The only advantage of selecting this working fluid for an air-air-cooled system over a water-water-cooled VCC—ORC is its higher net electricity value and ORC thermal efficiency. The net electricity value for an air-air-cooled VCC—ORC system varies from 0.468 kW to 0.380 kW. In contrast, a water-water-cooled VCC—ORC system decreases from 0.281 kW to 0.268 kW. In contrast, for an air-air-cooled system, the value of ORC thermal efficiency varies from 8.11 % to 7.32 %, and for a water-water-cooled system, it varies from 7.62 % to 7.44 % as the condensing air mass flow rate of ORC condensing air is varied from 3 kg/s to 11 kg/s. So, the water-water-cooled VCC—ORC system using R407c-R141b is better in terms of standalone COP_{VCC} and system COP, but the air-air-cooled VCC—ORC system using R410a-R141b is better if performance parameters of net electricity output and ORC thermal efficiency are considered. The reason is that for the same working conditions applied to the VCC system (i-e, cooling capacity, indoor air temperature, chilled water temperature, and mass flow rate), the water-air cooled system attains higher VCC evaporation temperature, and the compressor discharge temperature reduces due to which the net compressor work in case of water-air cooled system decreases and hence COP_{VCC} increases. Whereas in the case of an air-air-cooled system, the system attains lower VCC evaporation temperature and higher compressor discharge temperature, and as a result, the net compressor work increases, and COP_{VCC} will be decreased. In other words, the pressure ratio for a water-water-cooled system is slightly less than that of the air-air-cooled VCC—ORC system, which means that the COP_{VCC} is better for the water-water-cooled VCC—ORC system. The comparison of standalone COP of the VCC system, system COP, VCC evaporation and compressor discharge temperatures, and pressure ratio of VCC for air-air cooled and water-air cooled VCC—ORC system is shown in Fig. 14(c) and (d). The air-air-

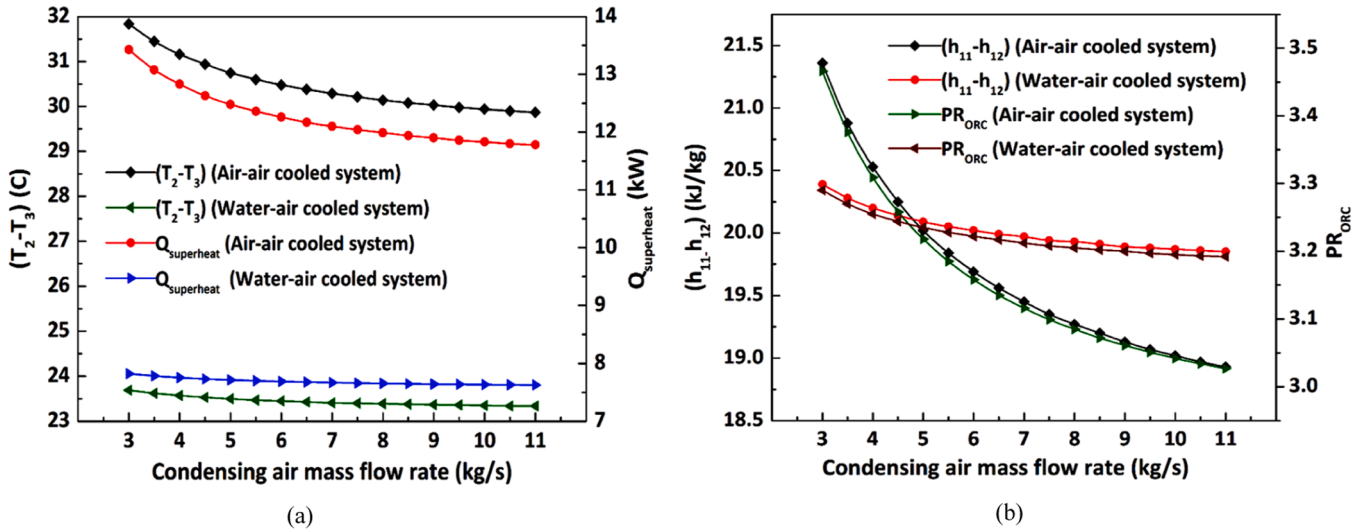

Fig. 15. Condensing air mass flow rate vs (a) (T_2-T_3) and $Q_{superheat}$ (b) Expander enthalpy difference and PR_{ORC}.

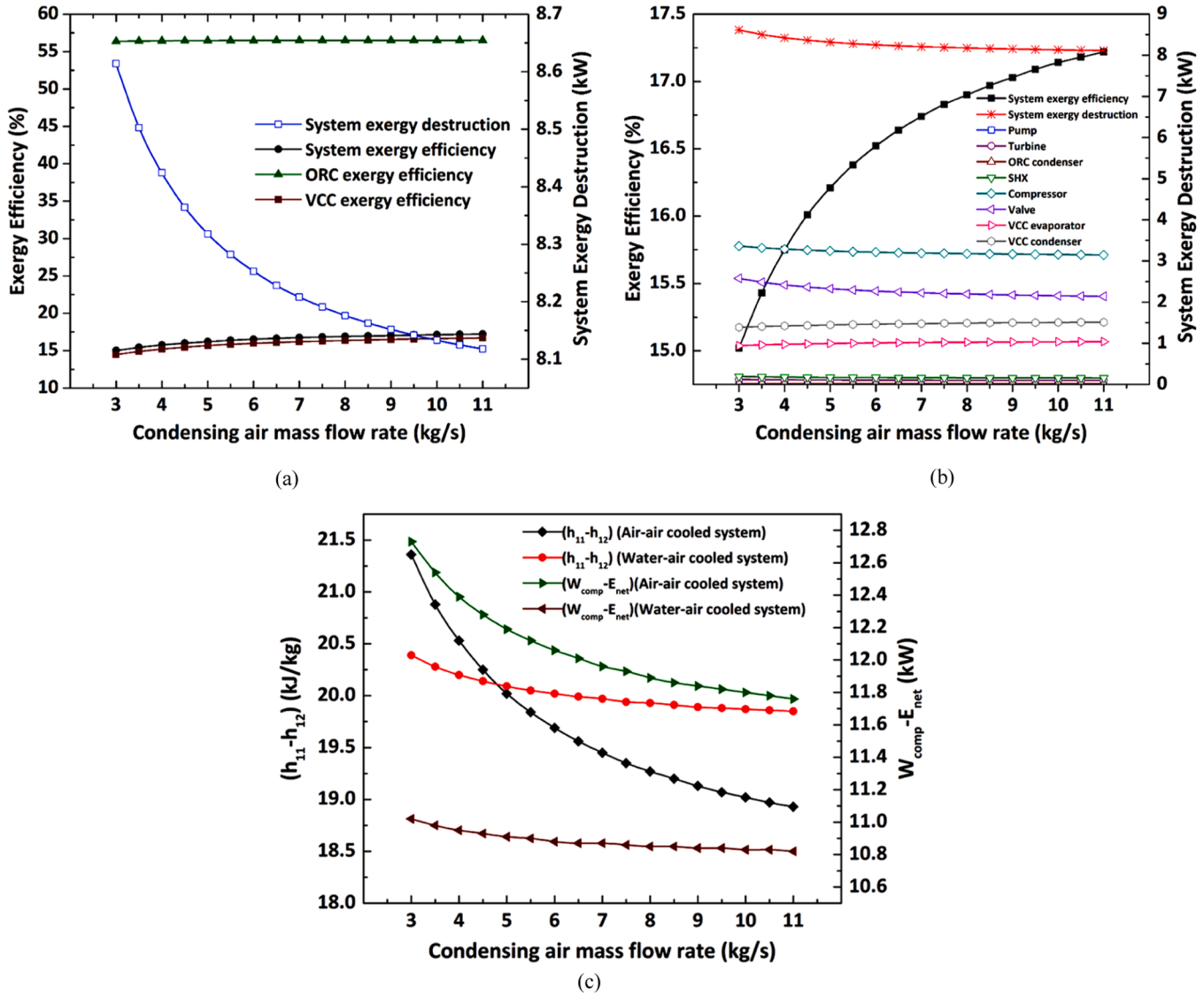

Fig. 16. Condensing air mass flow rate vs.(a)Exergy efficiency and System exergy destruction (b) Components exergy efficiency and Components exergy destruction (c)Expander enthalpy difference and (W_{comp}-E_{net}).

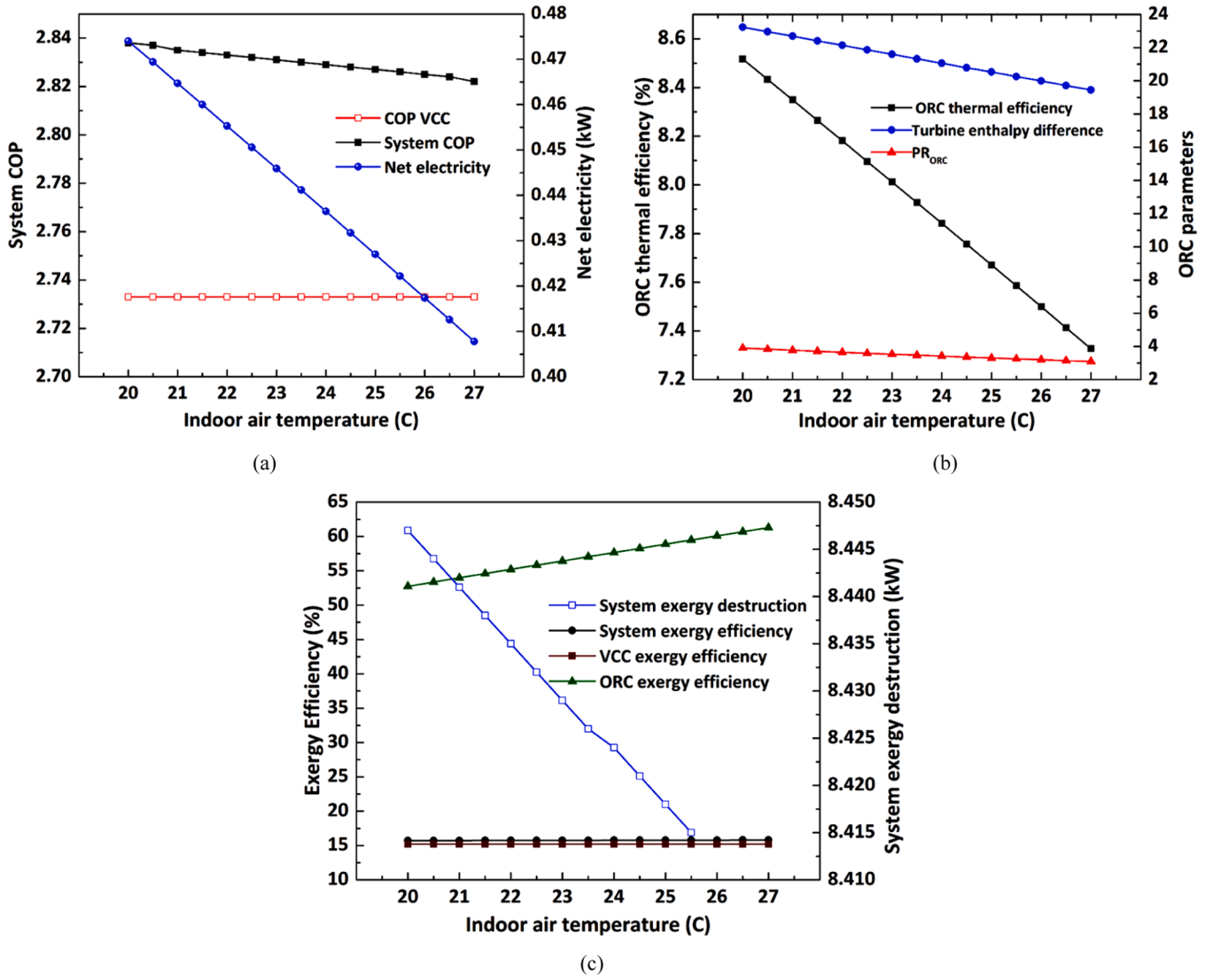

Fig. 17. Indoor air temperature vs (a) System COP and net electricity (b) ORC thermal efficiency, expander enthalpy difference, and PR_{ORC} (c) Exergy efficiency and System exergy destruction.

cooled system achieves the VCC evaporation of 2.21 °C and decreases to 1.72 °C as the ORC condensing water mass flow rate changes from 3 kg/s to 11 kg/s. Similarly, the compressor discharge temperature decreases from 83.35 °C to 77.03 °C within the same range of ORC condensing air mass flow rate. However, for water-air cooled system, VCC evaporation and compressor discharge temperature varies from 6.04 °C to 5.99 °C and 75.80 °C to 74.49 °C. The pressure ratio of VCC for an air-air-cooled system shows high values as compared to the water-water-cooled system. At ORC condensing water mass flow rate of 4 kg/s, the standalone COP and system COP values for air-air cooled system are 2.73 and 2.83, whereas for water-air cooled system, the values for the same performance parameters at 4 kg/s are 3.12 and 3.20 respectively.

Similarly, the trend of net electricity output and ORC thermal efficiency for the air-air-cooled system is also shown in Fig. 13(a) and (b). The net electricity generated by the system is higher than that generated by the water-air cooled system because of its higher temperature difference between the compressor discharge temperature and saturated vapour temperature at the VCC condenser (T_2-T_3). Due to this, the amount of superheat availability in case of an air-air-cooled system increases, ensuring more heat supply to the ORC system. Secondly, with the increase in ORC condensing air mass flow rate, the overall ORC condensing and evaporation temperature of an air-air-cooled system is higher than that of a water-water-cooled system. Due to this, the overall pressure ratio variation for an air-air-cooled system is and more significant than that of a water-water-cooled system. Therefore, the net enthalpy drop across the expander increases as the pressure ratio increases, and more work output will be obtained. The variation is also shown in Fig. 15(a) and (b).

Fig. 16 represents the exergetic performance of the air-air-cooled system. The VCC, ORC and system exergy efficiency increases with increasing ORC condensing air mass flow rates similar to the case described for a water-air cooled system. Overall, the water-water-cooled system using R407c-R141b in an integrated VCC—ORC system shows better exergetic efficiency than the air-air-cooled system using R410A-R141b. However, the increasing trend for both cases has been observed as the mass flow rate of the ORC condensing air has increased. The VCC and system exergy efficiency for air-air cooled systems increases from 14.48 % to 16.68 % and 15 % to 17.21 %, whereas the ORC exergy efficiency almost remains the same or increases very little at 55.1 % to 55.2 %. As mentioned, the VCC, ORC, and system exergy efficiencies are functions of mass flow rates, W_{comp}, and E_{net}. So, the increase in the compressor work is more in the case of the air-air cooled system for R410a-R141b as compared to the water-air cooled system using R407c-R141b as shown in Fig. 14(c) therefore, the overall increase in

the VCC exergy efficiency for air-air cooled system is less as compared to the water-air cooled system for the same range of changing ORC condensing air mass flow rate. Similarly, for system exergy efficiency, the factor ($\dot{W}_{comp} - \dot{E}_{net}$) for the air-air cooled system is more as compared to the water-air cooled system due to which the overall system COP for the water-air cooled system is more as compared to the air-air cooled system. In addition, due to greater enthalpy differences across expanders in air-air-cooled systems, the net electric work output is higher, which is why this system is preferred for net electricity production and overall ORC thermal efficiency. At ORC condensing mass flow rate of 4 kg/s, the value of VCC, ORC, and system exergy efficiency values for air-air cooled systems are 15.22 %, 55.12 %, and 15.74 %, respectively, whereas ORC thermal efficiency and net electricity values are 7.67 % and 0.43 kW respectively. At the same ORC condensing water mass flow rate of 4 kg/s, the air-air-cooled system had a 35 % and 1.43 % increase in net electricity output and ORC thermal efficiency compared to the water-water-cooled system. The variation for expander enthalpy difference and ($\dot{W}_{comp} - \dot{E}_{net}$) for air-air and water-air cooled systems is shown in Fig. 16(c).

5.2.3. Effect of indoor air temperature

If the indoor air temperature changes, the system's thermodynamic parameters will also be affected by the VCC parameters being fixed. This section will analyze the effect of varying the indoor air temperature from 20 °C to 27 °C and its thermodynamic impact on the air-air-cooled integrated VCC—ORC system. The VCC evaporation and condensation temperature will be fixed at 2 °C and 50 °C, which means the pressure ratio for the VCC cycle is fixed. Moreover, the cooling capacity and compressor discharge temperature will also remain the same. The amount of waste heat rejection from the VCC cycle remains the same at fixed VCC conditions. At these conditions, the value of the $Q_{superheat}$ rejected by the VCC cycle is 12.83 kW. Moreover, the ORC evaporation temperature is also fixed at 64 °C. The ORC condensing water mass flow rate is kept constant at 4 kg/s. According to the assumption, if the cooling fluid in the ORC condenser is air, the cooling fluid temperature equals the indoor air temperature. If the working fluid in the ORC condenser is other than air (water), then the ORC condensing temperature will be fixed at 30 °C. Since the ORC condenser is cooled by air, the ORC condensing temperature should be determined and dependent on indoor air temperature. So, as the indoor air temperature increases, the ORC condensing temperature will also increase at the fixed UA value of the ORC condenser. Since the ORC evaporator temperature is fixed, the increase in the ORC condensing temperature will decrease the enthalpy difference across the expander, and the pressure ratio of the ORC system will also decrease. Therefore, the net electricity output will be decreased. Secondly, as the $Q_{superheat}$ is fixed and the value of net electricity output decreases, the overall ORC thermal efficiency also decreases. The decrease in the net electricity output at increasing indoor air temperature also causes an increase in the value of ($\dot{W}_{comp} - \dot{E}_{net}$). This is because the VCC parameters are kept constant, so the compressor work will be the same. However, with the decreasing value of E_{net}, the overall value of ($\dot{W}_{comp} - \dot{E}_{net}$) increases, due to which the system COP decreases. The variation of the system COP, net electricity, expander enthalpy difference, and ORC pressure ratio with indoor air temperature is shown in Fig. 17(a) and (b). As mentioned above, the COP_{VCC} is maintained at 2.73 with fixed VCC cycle parameters. As the indoor air temperature increases from 20 °C to 27 °C, the value of ($\dot{W}_{comp} - \dot{E}_{net}$) increases from 12.35 kW to 12.41 kW, so the system COP decreases from 2.84 to 2.82. Whereas the net electricity output and thermal efficiency value also decrease as the expander enthalpy difference decreases and the ORC pressure ratio from 23.23 kJ/kg to 19.45 kJ/kg and 3.90 to 3.10, respectively. The exergetic performance of the air-air-cooled system with varying indoor air temperatures is also shown in Fig. 17(c). The VCC exergy efficiency remains at 15.22 % as cycle parameters are fixed, whereas the ORC exergy efficiency decreases from 61.30 % to 52.73 %. This is because as the indoor air temperature increases, the temperature of cooling ORC condensing air also increases, and the temperature difference increases, which decreases the heat transfer capability of the heat exchanger. Therefore, the overall exergy efficiency of the ORC system decreases. The overall exergy efficiency decreases very little, from 15.80 % to 15.72 %. This is because of the increase in the factor ($\dot{W}_{comp} - \dot{E}_{net}$), which increases from 12.35 kW to 12.41 kW; therefore, the system exergy efficiency decreases. The system exergy destruction of the air-air-cooled system decreases as the indoor air temperature increases to 25.5 °C. This is because the ORC mass flow rate increases from 0.217 kg/s to 0.2219 and ORC condensing temperature continue to decrease from 22.23 °C to 26.21 °C and the value of system exergy destruction decreases from 8.447 kW to 8.415 kW.

The cost of the heat exchangers, specifically the evaporator and condenser, significantly impacts the overall cost of the ORC system when utilizing a low-temperature heat source [44,45]. In the desuperheating approach, which involves recovering heat from the high-quality vapor in the superheated region, the heat transfer area is reduced due to higher temperatures, resulting in better thermal compatibility with the ORC working fluid. On the other hand, in the full recovery of heat rejection approach, the waste heat is recovered during the condensation of the VCC refrigerant, necessitating a larger heat transfer area for the evaporator and leading to higher exergy losses. From a thermo-economic perspective, the desuperheating method offers a lower investment cost than the full condensation method [31,46,47].

6. Conclusions

This work recovers the waste heat from the high-quality superheated region of the VCC cycle in the ORC cycle for electricity generation. A detailed thermodynamic analysis was conducted using two methods: cooling VCC and ORC condensers. The methods are termed as water-water and air-air-cooled integrated VCC—ORC systems. The performance evaluation and selection of the optimal working fluid have been conducted on a vapor compression system with a 10-ton (35 kW) refrigeration capacity (heat input).

Optimal Working Fluids and System Performance:

The desuperheating method is recommended to improve ORC thermal efficiency in water and air-air-cooled systems. The R407c-R141b fluid pair demonstrates superior performance for water-water-cooled systems with a system COP of 3.12, thermal efficiency of 7.56 %, and net electricity output of 0.28 kW. For air-air-cooled systems, the R410a-R141b pair achieves a thermal efficiency of 7.67 % and a higher net electricity output of 0.44 kW, making it the preferred choice for air-cooled applications.

Impact of Desuperheating:

The desuperheating method significantly improves ORC thermal efficiency in both systems, leveraging high-quality, high-temperature waste heat for electricity generation. The thermal efficiency reaches 7.56 % (water-water) and 7.67 % (air-air), highlighting the advantage of utilizing ultra-low-grade waste heat recovery potential.

Effects of Condensing Water Temperature:

Increasing condensing water temperature enhances net electricity and ORC thermal efficiency due to higher expander enthalpy and mass flow rates. However, it reduces COP, COP_{VCC}, and exergy efficiency due to increased exergy destruction.

Effect of Chilled Water Temperature in Water-Water System:

Higher chilled water temperatures in the water-water-cooled system improve COP and COP_{VCC} due to the decrease in the VCC pressure ratio and the factor ($\dot{W}_{comp} - \dot{E}_{net}$). This results in better system exergy efficiency, less exergy destruction, and higher system COP and COP_{VCC}.

Effect of Ambient Air Temperature in Air-Air System:

In the air-air-cooled system, increased ambient air temperature decreases system COP and net electricity output. A slight improvement in exergy efficiency and exergy destruction is observed up to 25.5 °C, but

Table 11
Thermal performance of optimal working fluid candidates.

Desuperheating Approach	Working fluid pair	COP_{VCC}	System COP	$\dot{E}_{net}$ (kW)	$\eta_{thermal}$ (%)	$\eta_{exergy,VCC}$ (%)	$\eta_{exergy,ORC}$ (%)	$\eta_{exergy,system}$ (%)	$\dot{I}_{total}$ (kW)
Water-water-cooled integrated VCC—ORC system	R407c-R141b	3.12	3.20	0.28	7.56	17.39	58.40	17.78	8.09
Air-air-cooled integrated VCC—ORC system	R410a-R141b	2.73	2.83	0.44	7.67	15.17	55.21	15.69	8.41

further temperature increases negatively impact performance.

Table 11 highlights the selection of optimal working fluids for both approaches, emphasizing the superior performance of R141b. This performance is primarily due to its higher latent heat of vaporization, which enables greater unit work output, and its lower ratio of latent heat of vaporization to sensible heat, which enhances thermal and exergy efficiency. Furthermore, the increased molecular complexity of R141b, as an isentropic fluid, significantly boosts both thermal efficiency and ORC exergy efficiency, making it an ideal choice for the system's performance optimization.

CRediT authorship contribution statement

Muhammad Asim: Writing – review & editing, Writing – original draft, Visualization, Validation, Software, Methodology, Investigation, Formal analysis, Data curation, Conceptualization. **Sheheryar Khan:** Writing – review & editing, Investigation, Formal analysis. **Shahid Ali Khan:** Writing – review & editing, Formal analysis, Data curation. **Taha Baig:** Writing – review & editing, Validation, Formal analysis, Data curation. **Muhammad Imran:** Writing – review & editing. **Abdul Wasy Zia:** Writing – review & editing, Visualization, Investigation. **Fahid Riaz:** Funding acquisition. **Michael K.H. Leung:** Writing – review & editing, Supervision, Software, Resources, Project administration.

Declaration of competing interest

The authors declare that they have no known competing financial interests or personal relationships that could have appeared to influence the work reported in this paper.

Acknowledgment

The work described in this paper was fully supported by a grant from the Research Grants Council of the Hong Kong Special Administrative Region, China (RGC Project Ref No.: UGC/FDS24/E12/24).

Data availability

No data was used for the research described in the article.

References

[1] F. Molés, J. Navarro-Esbrí, B. Peris, A. Mota-Babiloni, K. Kontomaris, Thermodynamic analysis of a combined organic Rankine cycle and vapor compression cycle system activated with low temperature heat sources using low GWP fluids, Appl. Therm. Eng. 87 (2015) 444–453, https://doi.org/10.1016/j.applthermaleng.2015.04.083.

[2] M. Imran, M. Usman, Y. Yang, B.-S. Park, Flow boiling of R245fa in the brazed plate heat exchanger: thermal and hydraulic performance assessment, Int. J. Heat Mass Transf. 110 (2017) 657–670, https://doi.org/10.1016/j.ijheatmasstransfer.2017.03.070.

[3] K.H. Kim, H. Perez-Blanco, Performance analysis of a combined organic Rankine cycle and vapor compression cycle for power and refrigeration cogeneration, Appl. Therm. Eng. 91 (2015) 964–974, https://doi.org/10.1016/j.applthermaleng.2015.04.062.

[4] W. Rattanongphisat, W. Rordprapat, Strategy for energy efficient buildings in tropical climate, Energy Proced. (2014) 10–17, https://doi.org/10.1016/j.egypro.2014.07.049.

[5] C. Li, J. Zhou, Y. Cao, J. Zhong, Y. Liu, C. Kang, Y. Tan, Interaction between urban microclimate and electric air-conditioning energy consumption during high temperature season, Appl. Energy 117 (2014) 149–156, https://doi.org/10.1016/j.apenergy.2013.11.057.

[6] D.K. Kim, J.S. Lee, J. Kim, M.S. Kim, M.S. Kim, Parametric study and performance evaluation of an organic Rankine cycle (ORC) system using low-grade heat at temperatures below 80°C, Appl. Energy (2017), https://doi.org/10.1016/j.apenergy.2016.12.026.

[7] H. Zhai, Q. An, L. Shi, V. Lemort, S. Quoilin, Categorization and analysis of heat sources for organic Rankine cycle systems, Renew. Sustain. Energy Rev. 64 (2016) 790–805, https://doi.org/10.1016/j.rser.2016.06.076.

[8] S. Quoilin, Sustainable energy conversion through the use of organic Rankine cycles for waste heat recovery and solar applications, English (2011).

[9] S. Baral, D. Kim, E. Yun, K. Kim, Energy, exergy and performance analysis of small-scale organic Rankine cycle systems for electrical power generation applicable in rural areas of developing countries, Energies 8 (2015) 684–713, https://doi.org/10.3390/en8020684.

[10] E. Yun, D. Kim, S.Y. Yoon, K.C. Kim, Experimental investigation of an organic Rankine cycle with multiple expanders used in parallel, Appl. Energy 145 (2015) 246–254, https://doi.org/10.1016/j.apenergy.2015.02.022.

[11] J. Jeong, Y.T. Kang, Analysis of a refrigeration cycle driven by refrigerant steam turbine, Int. J. Refrig. 27 (2004) 33–41, https://doi.org/10.1016/S0140-7007(03)00101-4.

[12] S. Aphornratana, T. Sriveerakul, Analysis of a combined Rankine-vapour-compression refrigeration cycle, Energy Convers. Manag. 51 (2010) 2557–2564, https://doi.org/10.1016/j.enconman.2010.04.016.

[13] H. Li, X. Bu, L. Wang, Z. Long, Y. Lian, Hydrocarbon working fluids for a Rankine cycle powered vapor compression refrigeration system using low-grade thermal energy, Energy Build. 65 (2013) 167–172, https://doi.org/10.1016/j.enbuild.2013.06.012.

[14] X. Bu, L. Wang, H. Li, Performance analysis and working fluid selection for geothermal energy-powered organic Rankine-vapor compression air conditioning, Geotherm. Energy 1 (2013) 1–14, https://doi.org/10.1186/2195-9706-1-2.

[15] B. Saleh, Parametric and working fluid analysis of a combined organic Rankine-vapor compression refrigeration system activated by low-grade thermal energy, J. Adv. Res. 7 (2016) 651–660, https://doi.org/10.1016/j.jare.2016.06.006.

[16] Z. Zhang, H. Su, G. Dai, X. Li, L. Zeng, Effects of variable-temperature heat reservoirs on performance of irreversible Carnot refrigerator with heat recovery, Sci. Rep. 13 (2023) 1–17, https://doi.org/10.1038/s41598-023-50011-9.

[17] J. Tang, L. Kang, Y. Liu, Automated configuration of organic Rankine cycle system based on process simulations, Energy Convers. Manag. 253 (2022) 115186.

[18] D. Prigmore, R. Barber, Cooling with the sun's heat Design considerations and test data for a Rankine cycle prototype, Sol. Energy 17 (1975) 185–192, https://doi.org/10.1016/0038-092X(75)90058-4.

[19] T. Ahamad, M. Parvez, S. Lal, O. Khan, M.J. Idrisi, 4-E analysis and multiple objective optimizations of a novel solar-powered cogeneration energy system for the simultaneous production of electrical power and heating, Sci. Rep. 13 (2023) 1–22, https://doi.org/10.1038/s41598-023-49344-2.

[20] K. Braimakis, S. Karellas, Energetic optimization of regenerative organic Rankine cycle (ORC) configurations, Energy Convers. Manag. 159 (2018) 353–370.

[21] M. Bahrami, F. Pourfayaz, A. Kasaeian, Low global warming potential (GWP) working fluids (WFs) for organic Rankine cycle (ORC) applications, Energy Rep. 8 (2022) 2976–2988.

[22] A.F. Babatunde, O.O. Sunday, A review of working fluids for organic Rankine cycle (ORC) applications, in: IOP Conf. Ser. Mater. Sci. Eng., IOP Publishing, 2018, p. 12019.

[23] E.I. Onyeocha, K.N. Nwaigwe, N.V. Ogueke, E.E. Anyanwu, Design and construction of an integrated tetrafluoroethane (R134a) refrigerator-waste heat recovery dryer for fabric drying in tropical regions, Heliyon 6 (2020) e04838, https://doi.org/10.1016/j.heliyon.2020.e04838.

[24] A.I. Papadopoulos, M. Stijepovic, P. Linke, On the systematic design and selection of optimal working fluids for organic Rankine cycles, Appl. Therm. Eng. 30 (2010) 760–769, https://doi.org/10.1016/j.applthermaleng.2009.12.006.

[25] M. Lampe, M. Stavrou, H.M. Bucker, J. Gross, A. Bardow, Simultaneous optimization of working fluid and process for organic Rankine cycles using PC-SAFT, Ind. Eng. Chem. Res. 53 (2014) 8821–8830, https://doi.org/10.1021/ie5006542.

[26] J. Schilling, M. Entrup, M. Hopp, J. Gross, A. Bardow, Towards optimal mixtures of working fluids: integrated design of processes and mixtures for organic Rankine cycles, Renew. Sustain. Energy Rev. 135 (2021) 110179.

[27] E. Wang, J. Mao, B. Zhang, Y. Wang, On the CAMD method based on PC-SAFT for working fluid design of a high-temperature organic Rankine cycle, Energy 263 (2023) 125935.

[28] E.C. Hohmann Jr, Optimum Networks For Heat Exchange, University of Southern California, 1971.

[29] M.T. Nasir, K.C. Kim, Working fluids selection and parametric optimization of an organic Rankine cycle coupled Vapor Compression Cycle (ORC-VCC) for air conditioning using low grade heat, Energy Build. 129 (2016) 378–395, https://doi.org/10.1016/j.enbuild.2016.07.068.

[30] M. Asim, M.K.H. Leung, Z. Shan, Y. Li, D.Y.C. Leung, M. Ni, Thermodynamic and thermo-economic analysis of integrated organic Rankine cycle for waste heat recovery from vapor compression refrigeration cycle, Energy Proced. 143 (2017) 192–198, https://doi.org/10.1016/j.egypro.2017.12.670.
[31] M. Asim, F. Kashif, J. Umer, J.Z. Alvi, M. Imran, S. Khan, A.W. Zia, M.K.H. Leung, Performance assessment and working fluid selection for novel integrated vapor compression cycle and organic Rankine cycle for ultra low grade waste heat recovery, Sustain 13 (2021) 11592, https://doi.org/10.3390/SU132111592.
[32] P. Zhao, J. Wang, L. Gao, Y. Dai, Parametric analysis of a hybrid power system using organic Rankine cycle to recover waste heat from proton exchange membrane fuel cell, Int. J. Hydrog. Energy 37 (2012) 3382–3391, https://doi.org/10.1016/j.ijhydene.2011.11.081.
[33] A.A. Lakew, O. Bolland, Working fluids for low-temperature heat source, Appl. Therm. Eng. 30 (2010) 1262–1268, https://doi.org/10.1016/j.applthermaleng.2010.02.009.
[34] A. Habibzadeh, M.M. Rashidi, N. Galanis, Analysis of a combined power and ejector-refrigeration cycle using low temperature heat, Energy Convers. Manag. 65 (2013) 381–391, https://doi.org/10.1016/j.enconman.2012.08.020.
[35] J. Bao, L. Zhao, A review of working fluid and expander selections for organic Rankine cycle, Renew. Sustain. Energy Rev. 24 (2013) 325–342, https://doi.org/10.1016/j.rser.2013.03.040.
[36] S.A. Klein, F. Alvarado, Engineering Equation Solver, F-Chart Softw, 2002, https://doi.org/10.1590/S1679-62252005000100009.
[37] O. Badr, P.W. O'callaghan, S.D. Probert, Vapour-compression Refrigeration Systems, 1990.
[38] B.F. Tchanche, G. Papadakis, G. Lambrinos, A. Frangoudakis, Fluid selection for a low-temperature solar organic Rankine cycle, Appl. Therm. Eng. 29 (2009) 2468–2476, https://doi.org/10.1016/j.applthermaleng.2008.12.025.
[39] Y. Feng, T. Hung, K. Greg, Y. Zhang, B. Li, J. Yang, Thermoeconomic comparison between pure and mixture working fluids of organic Rankine cycles (ORCs) for low temperature waste heat recovery, Energy Convers. Manag. 106 (2015) 859–872, https://doi.org/10.1016/j.enconman.2015.09.042.
[40] A.S.W. and D.Chisholm, Plate Heat exchangers: Plate Selection and Arrangement, AIChE Meet, Orlando, Florida, 1990. March 18-22.
[41] Y.Y. Hsieh, T.F. Lin, Saturated flow boiling heat transfer and pressure drop of refrigerant R-410A in a vertical plate heat exchanger, Int. J. Heat Mass Transf. 45 (2002) 1033–1044, https://doi.org/10.1016/S0017-9310(01)00219-8.
[42] Y.S. Kim, An Experimental Study on Evaporation Heat Transfer Characteristics and Pressure Drop in Plate Heat Exchanger, Diss. MS Thesis, Yonsei Univ, 1999.
[43] S. Quoilin, M. Orosz, H. Hemond, V. Lemort, Performance and design optimization of a low-cost solar organic Rankine cycle for remote power generation, Sol. Energy 85 (2011) 955–966, https://doi.org/10.1016/J.SOLENER.2011.02.010.
[44] S. Quoilin, S. Declaye, B.F. Tchanche, V. Lemort, Thermo-economic optimization of waste heat recovery organic Rankine cycles, Appl. Therm. Eng. 31 (2011) 2885–2893, https://doi.org/10.1016/j.applthermaleng.2011.05.014.
[45] F. Heberle, D. Brüggemann, Thermo-economic analysis of zeotropic mixtures and pure working fluids in organic Rankine cycles for waste heat recovery, Energies 9 (2016), https://doi.org/10.3390/en9040226.
[46] M. Asim, S. Khan, A.W. Zia, F.R. Siddiqui, M.K.H. Leung, Thermal performance enhancement of novel integrated vapor compression and organic rankine cycle for electricity production: a full-condensing vs. desuperheating approach comparison in ultra-low-grade waste heat recovery, E-Prime-Adv. Electr. Eng. Electron. Energy 7 (2024) 100493.
[47] M. Asim, M.K.H. Leung, Z. Shan, Y. Li, D.Y.C. Leung, M. Ni, Thermodynamic and thermo-economic analysis of integrated organic Rankine cycle for waste heat recovery from vapor compression refrigeration cycle, Energy Proced. (2017), https://doi.org/10.1016/j.egypro.2017.12.670.